minerals

MDPI

Review

Building an Orogen: Review of U-Pb Zircon Ages from the Calabria–Peloritani Terrane to Constrain the Timing of the Southern Variscan Belt

Annamaria Fornelli [1], Vincenzo Festa [1], Francesca Micheletti [1], Richard Spiess [2] and Fabrizio Tursi [1,*]

[1] Earth Science and Geo-Environmental Department, University of Bari Aldo Moro, via E. Orabona, 4, 70125 Bari, Italy; annamaria.fornelli@uniba.it (A.F.); vincenzo.festa@uniba.it (V.F.); francesca.micheletti@uniba.it (F.M.)

[2] Department of Geosciences, University of Padua, via G. Gradenigo 6, 35131 Padua, Italy; richard.spiess@unipd.it

* Correspondence: fabrizio.tursi@uniba.it

Received: 25 September 2020; Accepted: 22 October 2020; Published: 23 October 2020

Abstract: The application of zircon dating to the reconstruction of orogenic systems is invaluable since time constraints of the geological evolution of orogens are crucial for the proposal of geodynamic and paleogeographic models. Zircon is one of the most promising accessory minerals in geochronology of crystalline basements because of its high-closure temperature. Moreover, U-Pb data of relict and recrystallized grains indicate the maximum sedimentation age as well as the timing of metamorphism in metasediments. In addition, the U-Pb ages of magmatic zircons constrain the timescale of magmatism. The Calabria–Peloritani terrane (CPT) represents a key area in the Southern Variscan Belt, whose reconstruction is still unresolved. Therefore, a review of literature zircon age data accompanied with new data from six samples of orthogneisses, paragneisses, amphibolites, and actinolite schists, helps to constrain the evolution of this Cadomian fragment, affected by metamorphic and magmatic Variscan events. A revisiting of the timing of the geological events from Paleo-proterozoic to Permian is revealed by comparing the internal textures of zircons and their U-Pb age clusters. The detected age peaks at 2500 Ma, 1600 Ma, and 1000 Ma in the CPT were related to a provenance from West and East Gondwana realms. A sedimentation age around 630 Ma emerges for the middle-deep crust terranes of the CPT, affected by Ediacaran (579–540 Ma) intrusions, accompanied by metamorphism dated at 556–509 Ma in the host metasediments. In the following, during Ordovician–Silurian extensional tectonics, the former Cadomian terranes were at least locally affected by fluid-assisted metamorphism (around 450 Ma) whereas the upper extensional basins that formed, were infilled by sediments along with interspersed volcanic to subvolcanic products. All these pre-Silurian terranes were involved in the subduction process of the Palaeotethys–Gondwana margin beneath Laurussia. The compressive phase began around 347 Ma, with under-thrusting of the formerly Gondwana substrate that was subjected to middle-high grade metamorphism, while the Ordovician–Silurian sediments were scraped off along the front of the Southern Variscan Belt and affected by low-grade metamorphism. Decompression of the whole Variscan orogenic system started around 320 Ma, together with uplifting of the chain and emplacement of widespread granitic intrusions which ended around 280 Ma and completed the Variscan orogenic cycle in the CPT.

Keywords: U-Pb spot zircon ages; Gondwana metamorphic terranes; Ordovician–Silurian tectonics; Variscan orogen; Calabria–Peloritani

1. Introduction

Zircon is one of the most widespread accessory minerals in magmatic, metamorphic, and sedimentary rocks. Its excellent capacity to record the geological events makes it an indispensable tool for petrogenetic studies.

The ability of zircon to incorporate and retain trace elements such as Hf, U, Th, Y and rare earth elements (REE) as direct substitution into the Zr site [1] permits to evaluate the precise process of its formation and the timing of growth, using the U–Pb decay schemes. However, the U-Pb zircon ages must be accurately interpreted because several processes can disturb the U-Th-Pb systematics of crystals, such that the obtained ages can be without geological significance. The observations of habitus and internal zoning textures through Cathodoluminescence (CL), variable pressure secondary electron (VPSE), and back-scattered electron (BSE) images of zircon grains are essential for this issue, allowing the distinction among domains having igneous, metamorphic, detrital, or hydrothermal origin [2–6].

In the magmatic context, the regular oscillatory zoning is indicative of slow phase of growth from melt, while the euhedral crystals with development of 010 prism faces without internal structures, are generated by rapid growth in volcanic contexts (Figure 1a).

Obviously, these peculiarities may not be conclusive; therefore, only a large number of U-Pb spot analyses can constrain the timing and the context of the crystal growth and permit reliable dating of magmatic rock. Experimental data established the increase of the distribution coefficient of Heavy Rare Earth Elements (HREE) between zircon and melt ($Kd_{HREE}^{Zrn/Melt}$) with the decrease of temperature in the range 800–1050 °C at 20 kb in felsic rocks [6]; consequently, a HREE fractionated pattern of zircon can be assumed as typical of magmatic growth in acidic melts. Moreover, signatures of magmatic growth can also be derived from Th/U ratios being higher in magmatic zircon (i.e., Th/U > 1.0) [7]. Many exceptions are proposed for the chemical parameters defined earlier. One single parameter is not conclusive, but all the petrological, chemical, and structural observations contribute to the definition of the crystal origin.

More complex interpretations regard the ages of metamorphic zircons (Figure 1b). Homogeneous luminescent zircon rims without internal textures or perturbed crystals were related to metamorphic growth (Figure 1b) [2]. The challenge in metamorphic petrology is the dating of the single metamorphic phase in the pressure–temperature (*P–T*) evolution, hence, the partition of REE and the Th/U ratios of zircons become crucial. In granulitic terranes, garnet can be considered as a valuable "time marker" when associated with zircon [6,8]. Indeed, zircons with flat HREE pattern and Th/U ratio < 0.1 could be indicative of metamorphic growth synchronous with HREE-rich garnet competitor. However, a careful assessment of mineral parageneses (such as garnet and amphibole) coexisting with zircon at *P–T* conditions of amphibolite–granulite and eclogite facies [9,10], may help to constrain the *P–T–t* trajectories and to delineate the evolution of poly-metamorphic terranes [6,8,11–16]. Apart the growth from melt, also the interaction with a fluid phase under low grade metamorphic conditions might produce a resetting of U-Pb system of zircons [7]. Therefore, incoherent data ages (rim older than core) can be related to the opening of the U-Pb zircon system in which fluids played a role. Finally, hydrothermal fluids connected to magmatic intrusion can lead, in the surrounding rocks, to new zircon growth (Figure 1b, ZrnE), dating the magmatic emplacement event [17].

Zircons from poly-metamorphic terranes usually contain signatures of inherited grains (Figure 1b, Tur32-Zrn68); the careful dating and interpretation of relict grains contribute to define the origin of protoliths and, in favorable cases, the geological evolution of basement rocks from the depositional stage to the last metamorphic event. The opportunity to establish the sedimentation age of protoliths of metamorphic rocks was also used in the study of detrital zircons in sedimentary rocks (Figure 1c). Common applications of detrital zircon U-Pb ages include determination of sediment provenance, constrains of depositional age, reconstructions of dispersal sediment pathways [5,18], which are extremely useful in paleogeographic studies. The application of U-Pb dating of detrital zircons in volcanoclastic sandstones helps to define the age of deposition, synchronously with volcanic activity in sin-orogenic deposits where the remnants of fossils fail the precise dating [19–21].

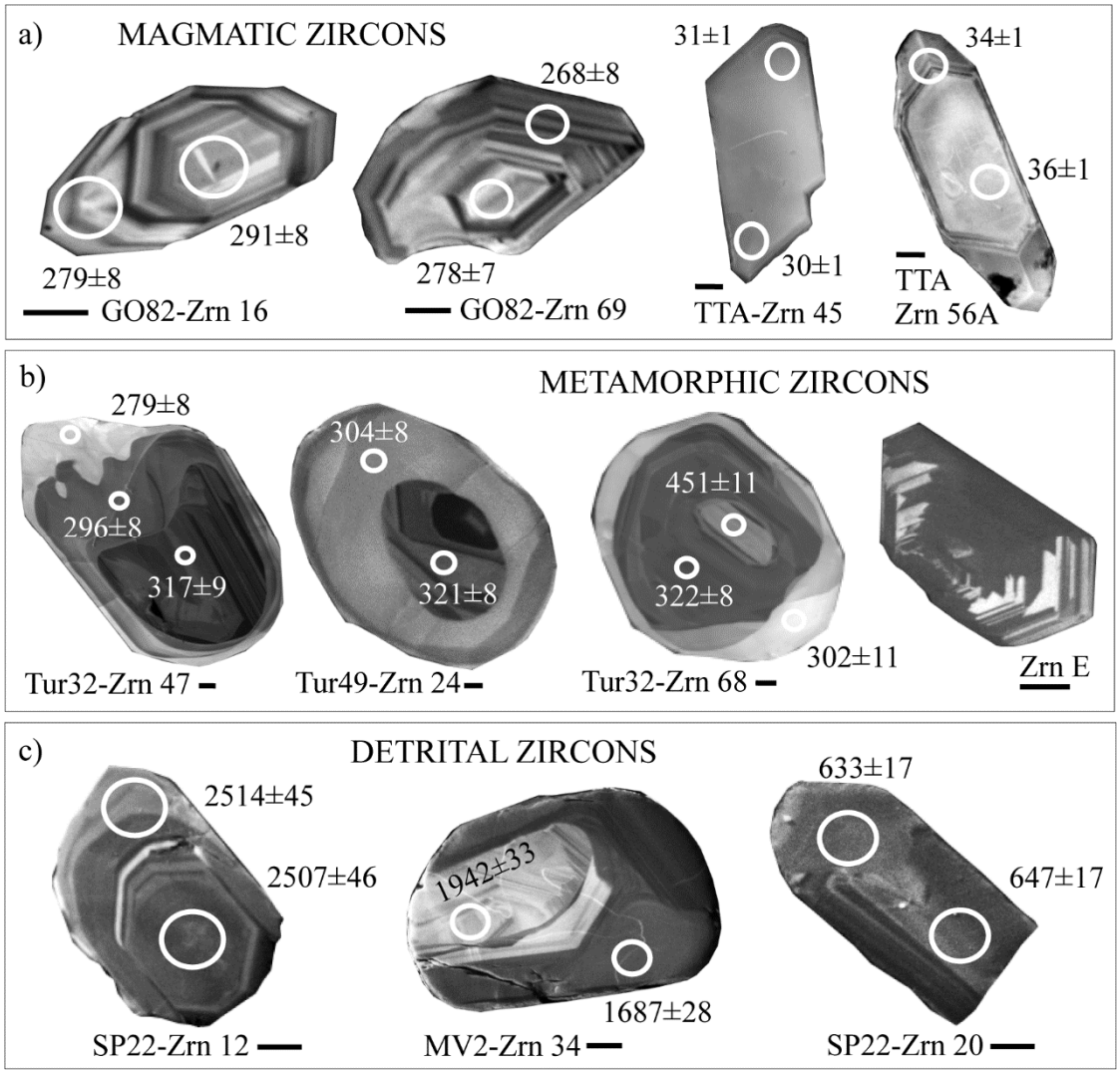

Figure 1. Typical internal zoning and textures of zircons having different genesis. (**a**) Zircon with magmatic oscillatory zoning in granitoids (Zrn16, Zrn69), modified from [17], CL images, and rapid growth in quite homogeneous luminescent volcanic zircons (Zrn45, Zrn56A), modified from [21], VPSE images. (**b**) Older cores of zircons showing younger and homogeneous overgrowths indicating multiple metamorphic crystallization, VPSE images: Zrn47 and Zrn24 modified from [8]; Zrn68, original; ZrnE modified from [7]. (**c**) Rounded, detrital zircons from sandstones, VPSE images: Zrn12 and Zrn20; Zrn34 modified from [22].

The brief summary of the applications and possible ambiguities of the U-Pb zircon dating highlights the greater complexity of age interpretations in metamorphic rocks since they may contain zircons inherited from metamorphic, magmatic, and sedimentary rocks and recrystallized crystals in one or more metamorphic events. A great challenge is to bring together, on a regional scale, the time evolution of crystalline rocks forming an orogenetic system.

A well-selected set of concordant zircon ages collected in different rock types forming the orogenic systems, allows the reconstruction of geological events of an orogen. The rock types of younger orogens may contain records that cover a wider age range than the orogenic cycle times, precisely these characteristics favor the paleogeographic reconstruction of the tectonic phases that lead to the formation of orogenic chains.

The power of zircon dating is used in this paper to present a review of spot U-Pb zircon data collected in the last 15 years from the metamorphic Calabria–Peloritani terrane (CPT) (southern Italy), in order to synthesize and link the large number of dating dispersed in several research papers. In particular, Ordovician ages are more and more frequent, and need to be interpreted in the framework of the peri-Gondwana terranes involved in the Southern Variscan Belt growth. The literature data

and new U-Pb zircon ages are presented to add more constraints for the magmatic, metamorphic, and sedimentary history, from Precambrian to Permian, of the CPT.

2. Geological Framework of the Calabria–Peloritani Terrane

Within the Apennine belt, which started to evolve during Oligocene, the CPT, i.e., the 'calabro-peloritano arc' sensu [23], is a stack of Eocene nappes characterized by both metamorphic rocks of the former Jurassic-Cretaceous Neo-Tethys oceanic crust and overlying metamorphic and intrusive rocks of Variscan continental crust derivation [24] (Figure 2).

The Variscan continental crust shows regional Carboniferous–Early Permian metamorphism, ranging from greenschists- to amphibolite- and granulite-facies [23,25]. A successive Eocene HP/LT metamorphism, related to the Alpine orogenic event [26–34], occurred primarily along ductile shear zones as the last overprinting event.

The largest nappe, both in terms of thickness and areal extent, is represented by the Sila–Serre Unit, and is well exposed in the homonymous massifs [35] (Figure 2). This unit includes a nearly complete but thinned late Variscan continental crust that is approximately 23 km thick [25,36] (Figure 2). The lower crustal level, equilibrated under granulite facies conditions, consists of metagabbros, mafic and felsic granulites, which are topped by migmatitic metapelites and metagreywackes with interbedded metabasite layers [8]. A thick batholith made up of Late Carboniferous–Early Permian granitoids occupies the mid-crustal level [37], while successions dominated by paragneisses or phyllites occur at the top, i.e., the so-called Mandatoriccio Paragneiss Unit and the Bocchigliero Phyllite Unit, in the Sila Massif, and the Mammola Paragneiss Unit and the Stilo–Pazzano Phyllite Unit, in the Serre Massif. The phyllite units and the underlying paragneiss ones were already tectonically juxtaposed, when the Late Carboniferous–Early Permian granitoids were intruding between the deep and the middle–upper crust [38–40]. The emplacement of the late Variscan granitoids determined a contact aureole in the middle–upper crustal levels, which was characterized by fluid-saturated or -undersaturated metamorphism near the batholith [41–45].

The paragneisses of the Mandatoriccio and Mammola units record lower amphibolite facies peak-pressure conditions at about 0.50 GPa [39,41] and about 0.85 GPa [45,46], respectively, which occurred during Upper Mississippian (i.e., 326 ± 6 Ma) regional metamorphism [41,45,47].

The Bocchigliero and Stilo–Pazzano units are largely characterized by phyllites, metarenites, metalimestones, and mafic and felsic metavolcanites, derived from a former Palaeozoic succession [48–51]. These units experienced low temperature greenschist facies regional metamorphism [38,50], dated at 330 ± 4 Ma (i.e., Upper Mississippian) in the Bocchigliero Phyllite Unit [52].

In the Sila and Serre massifs and in Catena Costiera, the Sila–Serre Unit rests above the Castagna Unit [33], which in turn tectonically overlies the phyllites of the Fiume Pomo Unit [53,54] (Figure 2). The Castagna Unit is dominated by orthogneisses (mostly augen gneisses), minor muscovite-leucocratic gneisses, paragneisses, actinolite schist, and amphibolites, that equilibrated under amphibolite facies at *P–T* conditions of about 0.3–0.6 GPa and 600–650 °C, during the Variscan orogeny [31,32]. Moreover, this unit is intruded by more or less deformed granitoids. According to [32], the homologue nappe of the Castagna Unit is represented by the Aspromonte–Peloritani Unit, which is exposed in the Aspromonte Massif and Peloritani Mountains. The Aspromonte–Peloritani Unit consists of orthogneisses (mostly augen gneisses), paragneisses, amphibolites, and marbles [55], intruded by Late Carboniferous–Permian granitoids [56]. It underlies the Stilo Unit of the Aspromonte Massif [57], that is composed by low greenschist- to amphibolite-facies metapelites [58] deriving from a former Paleozoic succession [59], and overlies a stack of nappes, among which the Variscan metamorphic rocks are included in the Mandanici Unit and the Lower Complex [29,60] (Figure 2). The Mandanici Unit is composed of phyllites and quartzites, with metabasites and calc-schists [61], while the Lower Complex consists of minor tectonic slices dominated by phyllites, porphyroids and metandesites, deriving from Palaeozoic volcano–sedimentary successions, equilibrated under low greenschists facies metamorphic conditions [62–64].

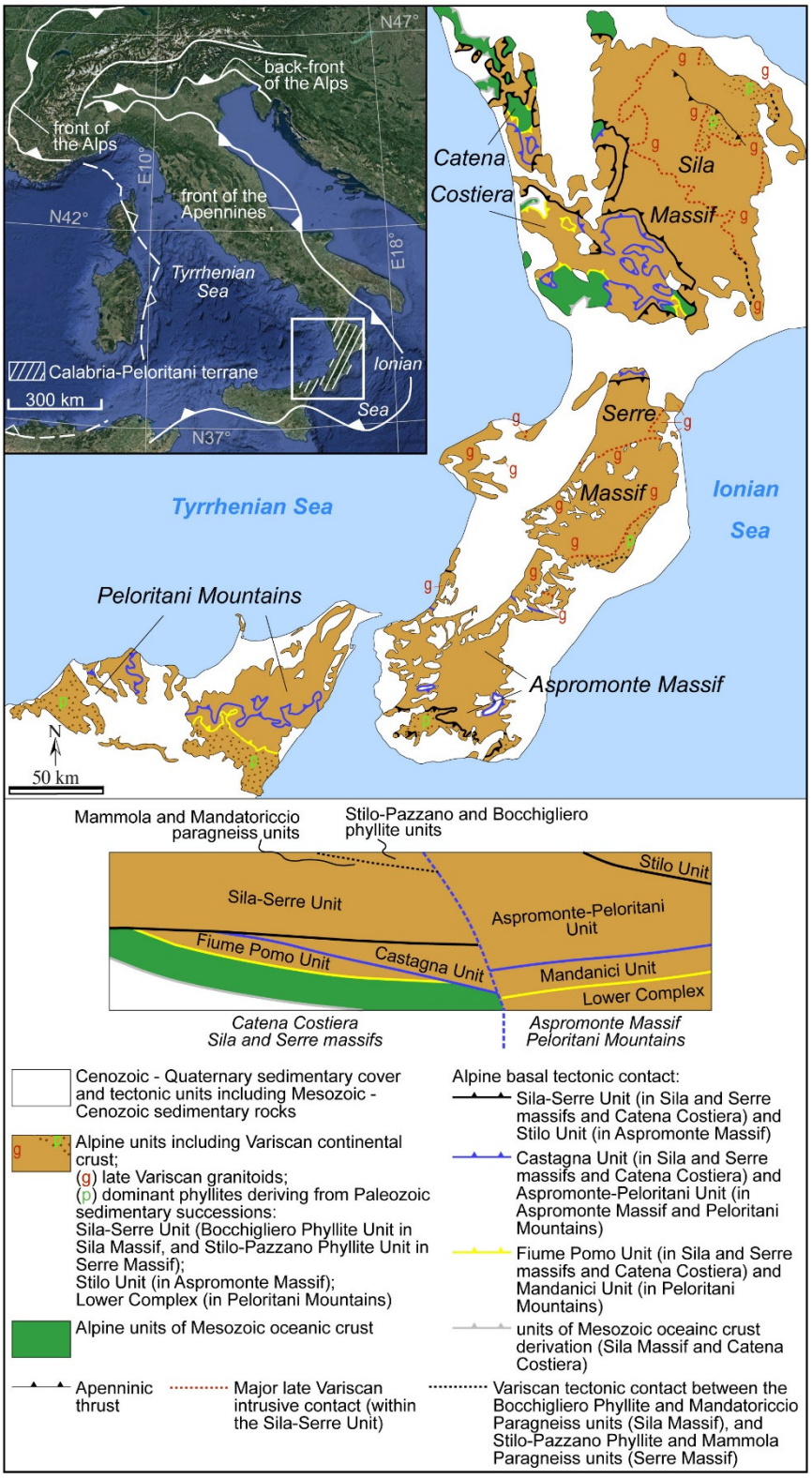

Figure 2. Structural sketch map (**above**) and 2D structural sketch (**below**), not to scale, of the CPT (modified from [35,56]).

3. Pre-Variscan Ages in the CPT

Records of Pre-Cambrian to Devonian magmatism, sedimentation, metamorphism, and anatexis are preserved in many tectonic units of the CPT, which were later subjected to Variscan orogeny [65]. Information on the pre-Variscan history of the CPT are provided by U-Pb zircon ages preserved in magmatic and metamorphic rocks belonging to the intermediate (i.e., the Castagna Unit, the

Mandatoriccio Unit, the Aspromonte–Peloritani Unit), the upper (i.e., the Lower Complex), and the deep crustal sectors (i.e., the deep crust of the Sila–Serre Unit) (Figure 2). These ages record the tectonic evolution of peri-Gondwana fragments already from Proterozoic. Records of these geological events are synthetized in the following, accompanied by new U-Pb zircon ages obtained for some crucial lithologies, with the aim of filling some literature gaps. The new U-Pb age data have been obtained on zircons from orthogneisses (AM1, FB1 samples), a paragneiss (GO59 sample), and an actinolite schist (GO176bis sample) of the Castagna Unit cropping out in Catena Costiera and Sila Massif (Figure 2), and from amphibolites (AS53, AS53bis samples) of the Aspromonte–Peloritani Unit cropping out in the Aspromonte Massif (Figure 2).

The analytical methods for the new U-Pb age data on zircon are detailed in the Appendix S1. The new U-Pb age data of analyzed zircons are reported as a supplementary data file (Table S1). A synthesis of the available literature data of zircon ages from all the CPT units mentioned above, along with the new age data we obtained, is shown in Table 1. In the following, the distribution of age data in the Castagna Unit, the Aspromonte–Peloritani Unit, the Lower Complex, and the Sila–Serre Unit is described.

3.1. Age Distribution in the Castagna Unit

According to the several dating carried out in the last 15 years on orthogneisses and muscovite-leucocratic gneisses of the Castagna Unit outcropping in the Sila Massif (Figure 2), their protolith ages have been tightly constrained in the Ediacaran, being 543 Ma and 540 Ma, respectively [17,66,67]. On the other hand, the distribution of zircon ages in their host rocks such as the paragneisses and the actinolite schists, and in the orthogneisses from Catena Costiera (Figure 2), was so far missing. New LA-CP-MS U-Pb zircon data were collected from a paragneiss sample (GO59) coming from the Sila Massif (39°01′27″ N Lat.; 16°33′25″ E Long.), an actinolite schist sample (GO176bis) coming from the Catena Costiera (39°08′58″ N Lat.; 16°06′28″ E Long.), and, in addition, two samples of orthogneiss intruded in metasediments from Catena Costiera were also analyzed. A complete U-Pb data set on zircons from these samples and relative Concordia diagrams are shown in Table S1 (Supplementary Materials), the most significant clusters are included in Table 1. Twenty-seven zircon grains from GO59 sample, produced 38 concordant ages covering a time span from 2085 ± 34 to 421 ± 6 Ma and 10 discordant ages. In GO176bis sample, 10 zircon grains gave 14 concordant ages from 2700 ± 38 to 596 ± 8 Ma and five discordant data. The new collected data from these samples are shown in Figure 3a.

Pre-Carboniferous age clusters can be recognized at 2686 ± 34 Ma, 2074 ± 33 Ma, 1651 ± 25 Ma, 1025 ± 18 Ma, 947 ± 13 Ma, 722 ± 14 Ma, 637 ± 9 Ma, 597 ± 12 Ma, 519 ± 12 Ma, and 452 ± 9 Ma. Variscan ages are missing. Ages older than about 519 ± 12 Ma were measured on zircon cores showing perturbed textures (Figure 3, GO176bis-Zrn3, GO59-Zrn12); in addition, ages clustering around 519 Ma and 452 Ma were obtained on resetted overgrowths (Figure 3, GO59-Zrn4b, GO59-Zrn12) holding, in some cases, the original oscillatory zoning (Figure 3, GO59-Zrn4).

The samples of orthogneiss were collected near Amantea village (AM1, 39°09′02″ N Lat.; 16°06′44″ E Long.) and in proximity of Fiumefreddo Bruzio village (FB1, 39°14′29″ N Lat.; 16°03′48″ E Long.) in Catena Costiera (Figure 2). The whole collected data on zircons are shown in Figure 3b. Twenty-one zircon grains from AM1 sample produced 26 concordant ages covering a time span from 1613 ± 28 to 504 ± 10 Ma and two discordant ages. The same number of zircon grains from FB1 sample gave 23 concordant ages from 587 ± 13 to 481 ± 11 Ma and a single discordant age.

Table 1. Concordant and subconcordant U-Pb data on zircon in the discussed Units from CPT. Subconcordant data ($^{206}Pb/^{238}U$ age) are indicated in italic. An upper intercept of discordia line in GO182 sample is indicated in italic bold.

Castagna Unit (Calabria)				
Sample & Mineral Assemblage	**Ages (Ma)**			
	Paleo-Proterozoic–Cambrian	**Ordovician–Silurian**	**Devonian**	**Carboniferous–Permian**
GO 59 paragneiss **(Sila Massif)**—This work (Qtz + Pl + Kfs + Bt ± Ms)	**2059 ± 32** (*n* = 3), 2085 ± 34, 2048 ± 30, 2045 ± 31, 1683 ± 25, 1619 ± 25, 1034 ± 28, 942 ± 12, 802 ± 21, **718 ± 15** (*n* = 4), 723 ± 9, 720 ± 17, 719 ± 17, 710 ± 16, 637 ± 9, 599 ± 16, 557 ± 14, 529 ± 14, 517 ± 14, 499 ± 12, 495 ± 6	**452 ± 9** (*n* = 19), 478 ± 12–421 ± 6		
GO 6 augen gneiss **(Sila Massif)**—[65] (Qtz + Kfs + Pl + Bt ± Ms)	2216 ± 56, 748 ± 6, 621 ± 5, 585 ± 5, 562 ± 5, 556 ± 5, **544 ± 5** (*n* = 5), 548 ± 5, 547 ± 4,543 ± 4, 542 ± 5, 541 ± 7, 515 ± 10	464 ± 4		
GO 35 augen gneiss **(Sila Massif)**—[65] (Qtz + Kfs + Pl + Bt ± Ms)	2069 ± 52, 588 ± 17, 566 ± 16, 556 ± 16, 552 ± 16, 544 ± 16			
GO 39 fine-grained leucocratic gneiss **(Sila Massif¤)**—[15] (Qtz + Kfs + Pl + Ms ± Bt)	858 ± 17, 632 ± 15, 631 ± 16, **533 ± 11** (*n* = 4)	473 ± 14, 459 ± 10, 413 ± 9		302 ± 12, 302 ± 8, 296 ± 9, 294 ± 8, 287 ± 9, 286 ± 7, 285 ± 7, 282 ± 7, 281 ± 7, 275 ± 8, 275 ± 7 (*n* = 2), 274 ± 8, 265 ± 6, 261 ± 6, 259 ± 11

GO 95 fine-grained leucocratic gneiss **(Sila Massif)**—[8] (Qtz + Pl ± Ms ± Kfs ± Bt)	801 ± 19, 633 ± 14, **547 ± 3** (*n* = 4), 521 ± 12, 509 ± 14, 504 ± 12, 494 ± 14	452 ± 13, 437 ± 10, 425 ± 11	**259 ± 4** (*n* = 6), 345 ± 9
GO 176bis actinolite schist **(Catena Costiera Massif)**—This work (Qtz + Kfs + Bt + Act ± Chl ± Ser)	2700 ± 38, 2671 ± 30, 2374 ± 35, 2116 ± 38, 1027 ± 13, 1013 ± 13, 970 ± 13, 928 ± 13, 865 ± 11, 856 ± 12, 741 ± 9, **638 ± 9** (*n* = 2), 638 ± 9, 637 ± 9, 596 ± 8		
FB1 augen gneiss **(Catena Costiera Massif)**—This work (Qtz + Kfs + Pl + Bt ± Ms)	587 ± 13, **533 ± 12** (*n* = 21), 563 ± 13 –507 ± 12	481 ± 11	
AM1 augen gneiss **(Catena Costiera Massif)**—This work (Qtz + Kfs + Pl + Bt ± Ms)	1613 ± 28, 973 ± 19, 758 ± 15, **580 ± 11** (*n* = 2), 580 ± 11, 579 ± 12, **531 ± 12** (*n* = 21), 552 ± 15 –504 ± 10		
	Aspromonte–Peloritani Unit		
ADR 5 augen gneiss **(Aspromonte Massif)**—[65] (Qtz + Kfs + Pl + Bt ± Ms)	917 ± 26, 614 ± 10, 611 ± 11, 597 ± 10, 586 ± 10, 577 ± 10, 568 ± 10, 566 ± 13, 550 ± 16, 527 ± 12		
ADR 18 augen gneiss **(Aspromonte Massif)**—[65] (Qtz + Kfs + Pl + Bt ± Ms)	623 ± 18, 617 ± 17, 565 ± 16, 548 ± 16, 531 ± 15, 526 ± 15, 522 ± 15	446 ± 13	
AS53-AS53bis amphibolite **(Aspromonte Massif)**—This work (Qtz + Kfs + Pl + Amph)	2463 ± 51, 2441 ± 50, 2225 ± 43, 2207 ± 45, 2080 ± 39, 1008 ± 17, 952 ± 16, 941 ± 13, 769 ± 10, 761 ± 13, 706 ± 10, 565 ± 8, 548 ± 7, 535 ± 10, 519 ± 9, 507 ± 7, 503 ± 6		391 ± 5, 368 ± 6
FIU-7 paragneiss **(Peloritani Mountains)**—[55] (Qtz + Bt + Pl ± Grt ± Sil)	**2668 ± 16** (*n* = 2), 2672 ± 9, 2664 ± 24,		

	2551 ± 16 (*n* = 3), 2586 ± 9, 2541 ± 14, 2525 ± 23, **2456 ± 37** (*n* = 8), 2493 ± 49–2424 ± 42, **1573 ± 42** (*n* = 2), 1585 ± 56, 1561 ± 28, 1123 ± 23, **1010 ± 15** (*n* = 4), 1022 ± 22–993 ± 9, **945 ± 12** (*n* = 6), 960 ± 12–930 ± 8, 904 ± 17, 855 ± 9, 852 ± 7, 835 ± 10, **768 ± 10** (*n* = 5), 782 ± 6–741 ± 4, 722 ± 30, **631 ± 7** (*n* = 9), 664 ± 9–611 ± 6, **546 ± 6** (*n* = 14), 566 ± 15–527 ± 5
FIU-11 augen gneiss **(Peloritani Mountains)**—[55,60] (Qtz + Kfs + Pl + Bt ± Ms ± Sil)	3242 ± 13, 2627 ± 25, 2534 ± 27, 1796 ± 35, 1022 ± 3, 958 ± 17, 810 ± 10, 767 ± 15, 728 ± 17, 642 ± 4, 630 ± 6, 610 ± 6, 607 ± 5, 578 ± 10, **545 ± 4** (*n* = 22), 558 ± 4–516 ± 4
MV-15 augen gneiss **(Peloritani Mountains)**—[55,60] (Kfs + Qtz + Pl + Bt ± Ms)	2455 ± 9, 2453 ± 39, 2210 ± 22, 1798 ± 30, 960 ± 8, 942 ± 12, 927 ± 10, 731 ± 8, 718 ± 8, 698 ± 8, 691 ± 11, 634 ± 14, **541 ± 5** (*n* = 25), 557 ± 6–528 ± 7
TC-9 augen gneiss **(Peloritani Mountains**—[60] (Kfs + Qtz + Pl + Bt)	581 ± 3–528 ± 4 (*n* = 35)

		Lower Complex		
Ta-Pu1-2-3, Ta-Cs, Tao Felsic porphyroids and andesites **(Peloritani Mountains)**—[61] *ID-TIMS data* (Qtz + Kfs ± Bt ± Ms ± Chl)	2013 ± 1, 1140 ± 10	**450 ± 12** (*n* = 16), 461 ± 10–432 ± 15	401 ± 20, 367 ± 13	
		Sila–Serre Unit (deep continental crust)		
Tur 3 restitic metagreywacke **(Serre Massif)**—[66] (Grt + Pl + Opx + Amph + Bt)		483 ± 9		325 ± 9, 316 ± 9, 308 ± 9, **297 ± 4** (*n* = 4), 275 ± 8, 257 ± 7
GO 182 migmatitic metapelite **(Serre Massif)**—[66] (Qtz + Pl + Kfs + Sil + Bt + Grt ± Crd)	*654 ± 15*, ***1113 ± 10***	*496 ± 11*	395 ± 9	**280 ± 2** (*n* = 18)
Tur 17 felsic granulite **(Serre Massif)**—[66] (Qtz + Pl + Kfs + Grt ± Bt)	*1688 ± 36*, *585 ± 9*			329 ± 14, **286 ± 4** (*n* = 8), 249 ± 4
Tur 76A mafic granulite **(Serre Massif)**—[67] (Pl + Opx + Grt + Amph + Bt)	513 ± 9	466 ± 15, 436 ± 15, 434 ± 6, 413 ± 6		345 ± 4, 298 ± 10, 295 ± 9, 291 ± 6, 285 ± 17, 278 ± 6
Grt3 mafic granulite **(Serre Massif)**—[68] (Pl + Grt + Bt + Opx + Qtz + Kfs)				357 ± 11, **320 ± 10** (*n* = 8), 334 ± 12–300 ± 9
MFS 3 metagabbro **(Serre Massif)**—[66] (Pl + Amph + Opx + Cpx)	584 ± 24, 506 ± 21	453 ± 19	377 ± 5	263 ± 8, 231 ± 5, **282 ± 5** (*n* = 4)
Tur 49 meta-quartz-diorite **(Serre Massif)**—[10] (Pl + Opx + Cpx + Amph)	744 ± 20, 574 ± 18	457 ± 13, 438 ± 13	380 ± 11	**347 ± 3** (*n* = 10), **319 ± 3** (*n* = 7), **296 ± 4** (*n* = 5)
Tur 32 metabasite interleaved with felsic granulites **(Serre Massif)**—[10] (Opx + Pl + Bt)	593 ± 14, 564 ± 17	**454 ± 12** (*n* = 4), 483 ± 12, 464 ± 12, 451 ± 11, 418 ± 14	**370 ± 6** (*n* = 3)	**340 ± 7** (*n* = 2), **321 ± 3** (*n* = 9), **300 ± 3** (*n* = 6), 279 ± 8, 277 ± 7, 260 ± 6, 252 ± 8
Tur 46 metabasite interleaved with migmatitic metapelites **(Serre Massif)**—[10] (Opx + Pl + Bt + Amph)	609 ± 29, 537 ± 15, 505 ± 11		382 ± 9	**318 ± 5** (*n* = 2), **303 ± 4** (*n* = 4), **294 ± 4** (*n* = 3), 279 ± 10
GO 100 augen gneiss **(Serre Massif)**—[65] (Qtz + Kfs + Pl + Bt ± Ms ± Grt ± Sil)	2502 ± 19, 2404 ± 92, 1760 ± 46, 752 ± 6, 617 ± 23, 575 ± 4, 572 ± 6, 571 ± 4, 552 ± 9, 545 ± 4, 539 ± 7, 537 ± 4,	494 ± 14, 462 ± 7		

Garnet-biotite gneiss **(northern CPT)**—[69] (Pl + Qtz + Grt + Bt)	1789 ± 31, 1779 ± 31, 1111 ± 44–836 ± 19 (*n* = 12), 701 ± 24, 696 ± 17, 610 ± 16, 586 ± 17–513 ± 17 (*n* = 6)	475 ± 16, 457 ± 12	303 ± 8–297 ± 8 (*n* = 4) 280 ± 11, 255 ± 11
Sila–Serre Unit (Mandatoriccio Unit)			
LL61b2 micaschist **(Sila Massif)**—[70] (Bt + Grt + And + St + Ms ± Crd ± Sil)	2506 ± 43, 1948 ± 49, 1870 ± 41, 1637 ± 49, **1005 ± 26** (*n* = 6), 1024 ± 26, 1023 ± 24, 1018 ± 28, 1005 ± 33, 985 ± 28, 977 ± 19, 884 ± 21, 791 ± 25, 780 ± 28, 663 ± 19–585 ± 13, **622 ± 17** (*n* = 19), **524 ± 13** (*n* = 7), 547 ± 12–485 ± 13	**446 ± 12** (*n* = 7), 457 ± 12–428 ± 10	

Mineral abbreviations: Qtz: quartz; Pl: plagioclase; Kfs: K-feldspar, Grt: garnet, Bt: biotite, Ms: muscovite, Amph: amphibole, Crd: cordierite, Opx: orthopyroxene, Cpx: clinopyroxene, Sil: sillimanite, And: andalusite, St: staurolite. Means of concordant ages are indicated in bold.

A few Proterozoic ages at 1613 ± 28 Ma, 973 ± 19 Ma, and 758 ± 15 Ma represent inheritances (Figure 3b and Table 1), whereas the majority of the data (92%) are Proterozoic–Cambrian (587 ± 13 Ma, 504 ± 10 Ma, n = 45). They are grouped in three main clusters at 574 ± 12 Ma (n = 5), 540 ± 12 Ma (n = 23), and 518 ± 11 Ma (n = 17). The most frequent ages peaking at 540 ± 12 Ma seem related to the intrusion event of the orthogneiss protolith, as this age quite corresponds, within the error, with the emplacement age of the protoliths of the orthogneisses from other sectors of the CPT [61,66]. The age peak at 574 ± 12 Ma can be related to relict grains, whereas the significant cluster at 518 ± 11 Ma was measured on quite homogeneous luminescent rims (Figure 3b), suggesting a thermal perturbation successive to their intrusion, which also affected their host metasediments, that show the same age peak (cf Figure 3a,b). Variscan ages are missing as detected in the widespread augen gneisses of CPT.

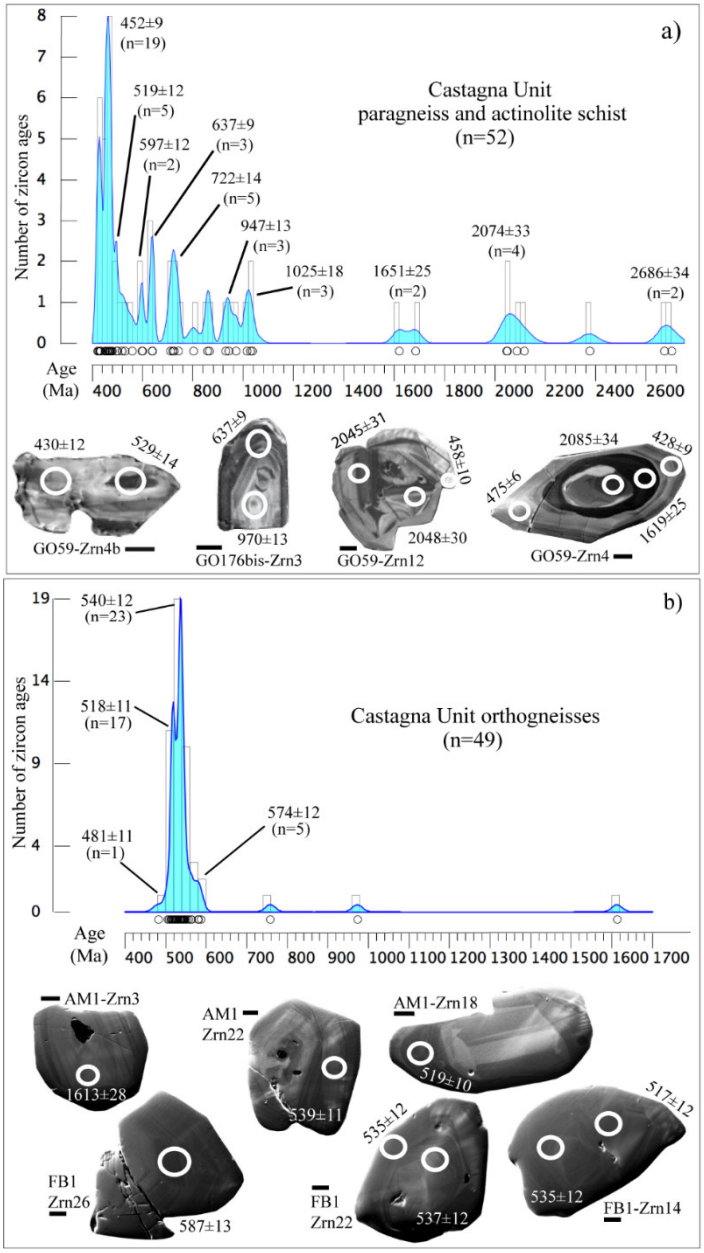

Figure 3. Histograms with probability density plot [68] of U-Pb zircon ages in paragneiss and actinolite schist samples (**a**), and orthogneiss from Catena Costiera (**b**) belonging to the Castagna Unit. Age clusters are indicated in correspondence of the peaks of the probability density plot. Spot ages on the selected zircons (VPSE images) reflect the age clusters shown in the histogram. The white circles on zircons represent the analyzed spots, the numbers show the ages in millions of years, the thick bar near the crystal label is 20 μm.

3.2. Age Distribution in the Aspromonte–Peloritani Unit

The protolith age of the orthogneisses of the Aspromonte–Peloritani Unit, was dated around 545 Ma by [56,61], with U-Pb systematics on zircons. Their host rocks are represented by paragneisses, which were dated through the same systematic by [55] in the Peloritani Mountains (Figure 2). We performed new U-Pb zircon dating (Table S1) from amphibolites (AS53 and AS53 bis samples, 37°55′40″ N Lat.; 15°58′30″ E Long.) interbedded within paragneisses in the Aspromonte Massif. Ten analyzed zircon grains gave 19 concordant ages covering a time span from 2463 ± 51 Ma to 368 ± 6 Ma and three discordant ages. The spectrum of new acquired data of the amphibolites is included with that of the paragneiss from [56,61] in Figure 4. Single zircon data of amphibolites are reported in Table S1 with relative Concordia diagrams. Age clusters of the amphibolite and paragneiss correspond to 2668 ± 16 Ma, 2455 ± 40 Ma, 2167 ± 36 Ma, 1573 ± 42 Ma, 1010 ± 16 Ma, 945 ± 13 Ma, 767 ± 10 Ma, 631 ± 7 Ma, 541 ± 6 Ma, and 380 ± 6 Ma. These age data correspond to inherited grains (Figure 4, Zrn13), some of these showing younger recrystallized domains around 541 ± 6 Ma (Figure 4, e.g., Zrn71). Most of the age peaks correspond to those detected in the previous units. Substantial differences are the missing of age peaks around 450 Ma and the presence of Devonian signature (Figure 4, Zrn3 dated at 391 ± 5 Ma).

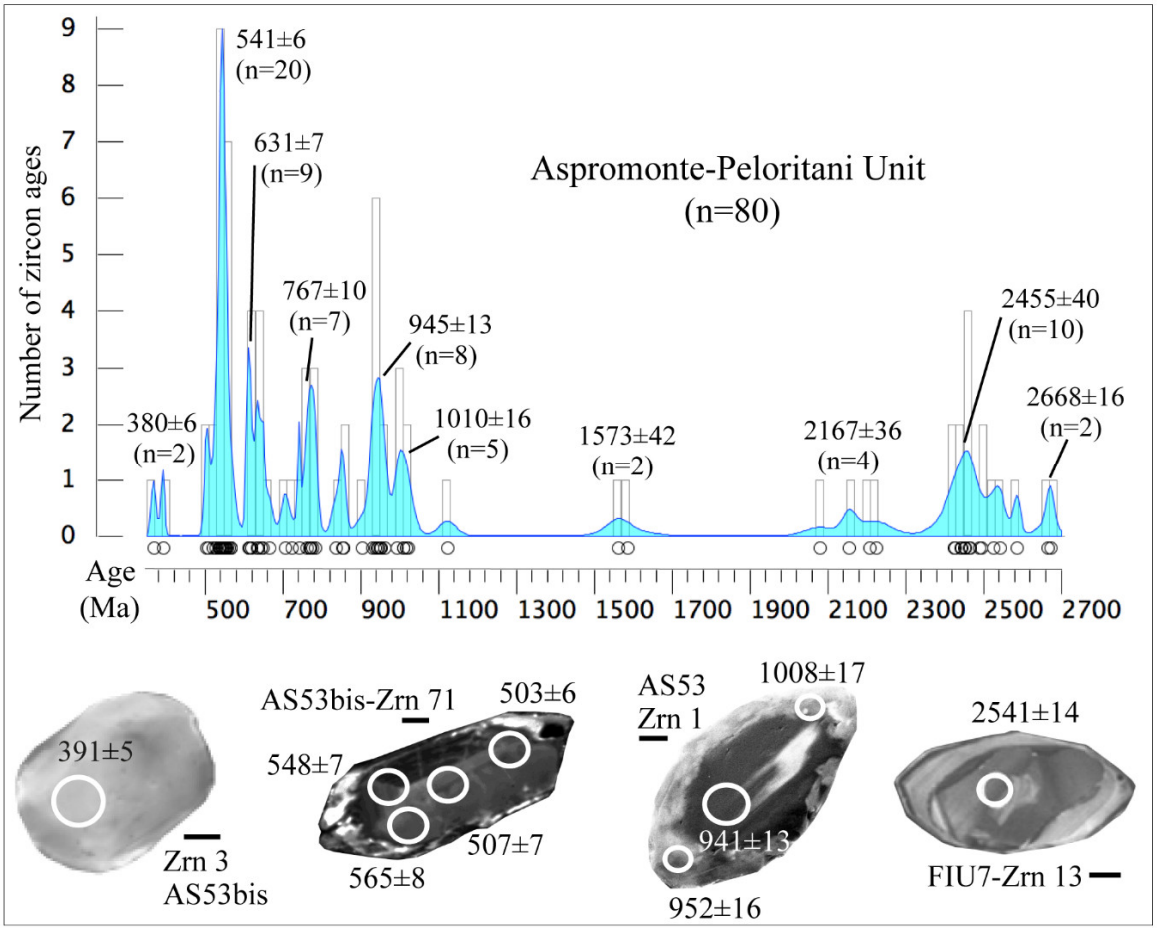

Figure 4. Histogram and probability density plot of zircon ages in paragneiss (CL image of FIU07-Zrn13 from [55]) and amphibolite (original VPSE images and ages of zircons from AS53 and AS53bis samples) from the Aspromonte–Peloritani Unit. Spot ages on the selected zircons (VPSE and CL images) are examples of the age clusters. Symbols as in Figure 3.

3.3. Age Distribution in the Lower Complex

Available U-Pb zircon ages from the literature were obtained from felsic porphyroids and meta-andesites interbedded with very low-grade metasediments of the Lower Complex cropping out in the Peloritani Mountains (Figure 2). The crystallization age of their protoliths was in the range of 461–

432 Ma [62], which was interpreted as volcanic–subvolcanic activity, synchronous with the deposition of the protoliths of the metasediments. However, inherited zircon ages corresponding to Paleo-proterozoic (2013 ± 1 Ma) and Meso-proterozoic (1140 ± 10 Ma) were also collected, together with younger Devonian ages of 401 ± 20 Ma and 367 ± 13 Ma [62] (Table 1).

3.4. Age Distribution in the Sila–Serre Unit

Many U-Pb zircon ages are available for the lower continental crust of the Sila–Serre Unit (i.e., mafic and felsic granulites, metagabbros, migmatitic paragneisses, metabasites, and orthogneisses) cropping out in the Serre Massif [8,66,69] (Figure 2) and in a garnet-biotite gneiss belonging to a Cenozoic tectonic melange near the northern border of the CPT [70], as well as for the paragneisses of the Mandatoriccio Paragneiss Unit [71]. U-Pb zircon data for the Mammola Paragneiss Unit and from low-grade metamorphic rocks of the Sila–Serre Unit (i.e., the Stilo–Pazzano Phyllite and the Bocchigliero Phyllite units) are missing.

The lower continental crust records an Ediacaran magmatism: protoliths of metagabbros were dated at ca. 579 Ma [70], whereas protoliths of augen gneisses were dated at ca. 543 Ma, similarly to other orthogneisses widespread in the CPT [55,61,65,66]. The age spectrum of high-grade metasediments and metabasites is shown in Figure 5. The pre-Carboniferous age peaks corresponding to 1784 ± 31 Ma, 992 ± 26 Ma, 714 ± 20 Ma (Figure 5) were detected on zircon cores. Ages around 649 ± 13 Ma were collected on relict core showing younger overgrowths (Figure 5, e.g., Zrn71, Zrn61d, Zrn18), while five relevant age peaks at 596 ± 19 Ma, 556 ± 16 Ma, 509 ± 15 Ma, 452 ± 12 Ma, and 375 ± 10 Ma were obtained on probably metamorphic recrystallized zircons (Figure 5, e.g., Zrn61d, Zrn2).

As regards the Mandatoriccio Paragneiss Unit, many U-Pb age data on zircon were collected on paragneiss of this unit by [71]. The age clusters shown in Figure 6 evidence peaks at 2506 ± 43 Ma, 1909 ± 45 Ma, 1637 ± 49 Ma, 1005 ± 26 Ma, 786 ± 27 Ma, 622 ± 17 Ma, 524 ± 13 Ma, and 446 ± 12 Ma. Oscillatory zoning and homogeneous textures of the dated zircons were interpreted by [70] as indicative of magmatic and metamorphic origin, respectively. The age clusters in these paragneisses were interpreted as indicative of the ages of the source rocks, and the youngest ages (about 446 ± 12 Ma) were considered as the maximum sedimentation age [72,73]. However, a network of bright veins characterizes crystals dating around 450 Ma (Figure 6, Zrn28A), suggesting that such zircons may have been perturbed.

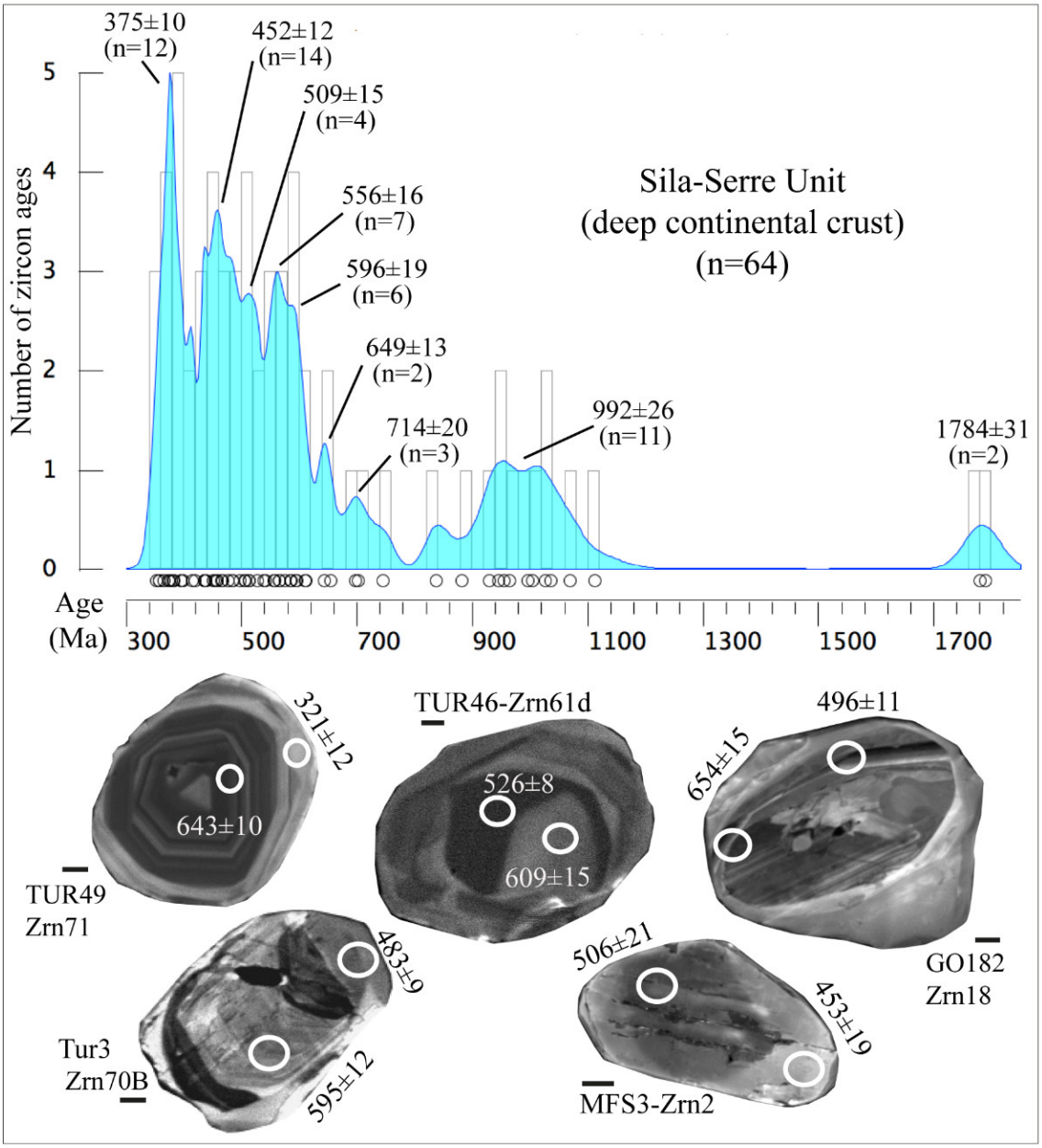

Figure 5. Histogram and probability density plot of zircon ages in metagabbro, metabasite, meta-quartz-diorite, migmatitic metapelite, restitic metagreywacke, mafic and felsic granulite from the deep crust of the Sila–Serre Unit. Spot ages on the selected zircons (VPSE and CL images) reveal the age clusters (modified after [8,65,69]); note the younger metamorphic overgrowths on older relict zircons. Symbols as Figure 3.

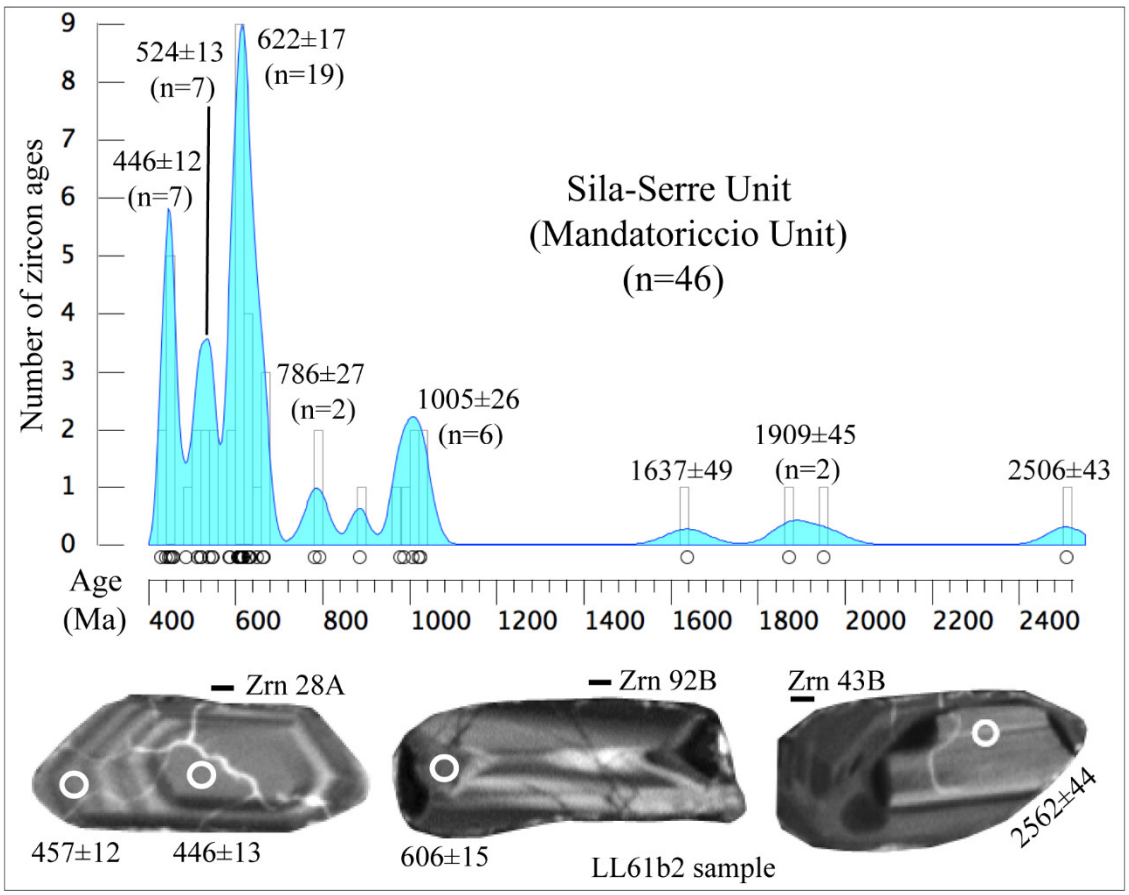

Figure 6. Histogram and probability density plot of zircon ages in paragneiss from the Mandatoriccio Unit (data from [71]). Spot ages in the selected zircons (CL images) reflect the main age clusters. Note the network of bright veins affecting Zrn28A. Zircons 28A, 92B, and 43B are modified after [70]. Symbols as in Figure 3.

4. A Synthesis of the Variscan Ages

The Carboniferous–Permian ages of zircons from metasediments, orthogneisses, metabasites, and granitoids regard the timing of Variscan metamorphism and magmatism. However, because the ability of zircon to record the metamorphic events depends mostly on temperature (e.g., [74,75]), the correlation between zircon ages and the timing of the main metamorphic events was only possible for high-grade metamorphic rocks of the lower continental crust of the Sila–Serre Unit. More in detail, dating was largely carried out on felsic and mafic granulites, including layered metagabbros, along with interspersed metaperidotites, restitic metasediments and the overlying migmatitic metapelites, metagreywackes, metabasites, and orthogneisses, as all these rocks experienced different degrees of partial melting during the Variscan orogeny [76,77]. However, also some muscovite-leucocratic gneisses of the Castagna Unit record some Variscan ages, the latter related to intense, late-Variscan hydrothermal fluid activity [17].

The Variscan age spectrum of zircons from the lower continental crust of the CPT covers a range from 357 ± 11 to 231 ± 5 Ma (Figure 7).

Moving from older ages (Figure 7), a first consistent cluster of U-Pb ages (n = 10) occurs at 347 ± 10 Ma in four samples of mafic granulites (cf. Table 1), which is related either to poorly zoned crystals or structureless poorly luminescent cores (Figure 7, e.g., Tur49-Zrn29, Tur49-Zrn7) whereas, a second, more pronounced age cluster, occurs at 321 ± 9 Ma, obtained on perturbed and poorly luminescent domains (Figure 7, e.g., Tur49-Zrn60). According to [8], the Variscan zircon domains dated at about 347 Ma show flat HREE patterns and low Eu/Eu* ratios, indicating a synchronous growth with strong competitors such as garnet and plagioclase, respectively [6]. According to [77], ages around 347 Ma date the stage of prograde metamorphism during crustal thickening. The age group at about 321 Ma

represents the beginning of decompression of the lower continental crust in which multistage partial melting events occurred [76]. Moreover, the U-Pb age of magmatic zircons from a quartz-monzodioritic dike intruded within the lower continental crust, were dated at 323 ± 5 Ma by [77,78], and interpreted as the beginning of the Variscan magmatism in the Serre Massif [78]. In addition, small trondhjemitic plutons were emplaced at around 314 Ma as evidenced by U-Pb zircon ages in Aspromonte–Peloritani Unit [79,80].

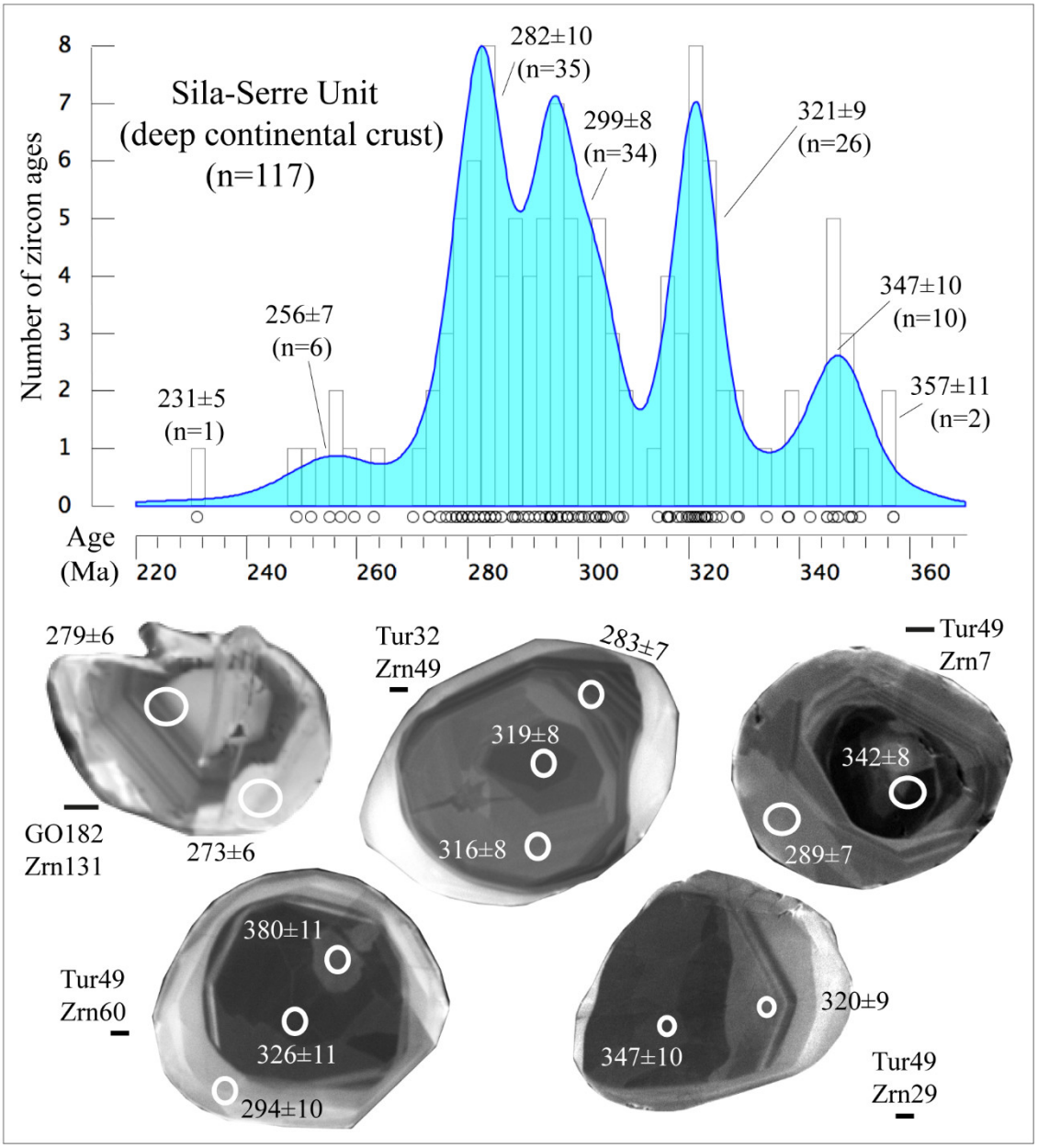

Figure 7. Histogram and probability density plot of prevalent Carboniferous zircon ages [8,69] and related clusters in the deep crust of the Sila–Serre Unit. Spot ages in the selected zircons (CL and VPSE images) denote the age clusters related to the different metamorphic stages (Zrn131 modified after [69], original images for Zrn49, Zrn7, Zrn60, and Zrn29). Data ranging from about 326 Ma to about 273 Ma are connected to Carboniferous emplacement of granitoids. Symbols as in Figure 3.

Other two consistent clusters of U-Pb zircon ages were determined for the high-grade metamorphic rocks of the lower continental crust of the Sila–Serre Unit (Figure 7): (i) at 299 ± 8 Ma, measured on grey and homogeneous rim domains (Figure 7, e.g., Tur49-Zrn60); (ii) at 282 ± 10 Ma (Figure 7, e.g., Tur32-Zrn49, GO182-Zrn131) obtained on homogeneous rims.

The cluster at around 299 Ma was interpreted by [77] as the main decompression phase under isothermal conditions which culminated with widespread partial melting events, involving the most fertile source rocks, such as the metapelites in the upper portion of the lower continental crust [76]. This age broadly overlaps with the cooling ages of 292–297 Ma and 293 ± 2 Ma measured on the granitoids by [79,81] and [37,82], respectively, signing the intrusions of huge masses of granitoids forming the batholith exposed in the Sila and Serre massifs. Finally, some ages around 282 Ma (Figure 7) were determined on zircons which show fractionated HREE patterns connected to garnet absence [8]; this age was interpreted as the end of the crustal decompression [69].

5. Discussion

Considering all pre-Carboniferous and Carboniferous–Permian U-Pb zircon dating from the CPT, our review of age data provides new insights for both the evolution of the northern peri-Gondwana, especially during Middle Ordovician–Upper Devonian, and its involvement in the Variscan orogeny. As shown in several probability density plots of zircon ages (Figures 3–6), the pre-Variscan orogeny signatures from the CPT are summarized in the comprehensive Table 2.

Table 2. Summary of the pre-Variscan age peaks from each discussed unit of the CTP (original and literature data as in Table 1).

Ages	Castagna Unit	Aspromonte–Peloritani Unit	Lower Complex	Sila–Serre Unit	
				Deep Continental Crust	Mandatoriccio Unit
Neo-archean–Paleo-Proterozoic	2686 ± 34 Ma; 2074 ± 33 Ma; 1651 ± 25 Ma	2668 ± 16 Ma; 2455 ± 40 Ma; 2167 ± 36 Ma	2013 ± 1 Ma	1784 ± 31 Ma	2506 ± 43 Ma; 1909 ± 45 Ma; 1637 ± 49 Ma
Stenian–Tonian	1025 ± 18 Ma; 947 ± 13 Ma	1573 ± 42 Ma; 1010 ± 16 Ma; 945 ± 13 Ma	1140 ± 10 Ma	992 ± 26 Ma	1005 ± 26 Ma
Cryogenian–Ediacaran	722 ± 14 Ma; 637 ± 9 Ma	767 ± 10 Ma; 631 ± 7 Ma		714 ± 20 Ma 649 ± 13	786 ± 27 Ma; 622 ± 17 Ma
Ediacaran–Cambrian	597 ± 12 Ma; 519 ± 12 Ma	541 ± 6 Ma		596 ± 19 Ma; 556 ± 16 Ma 509 ± 15 Ma	524 ± 13 Ma
Ordovician–Silurian	452 ± 10 Ma		461 ± 10 Ma; 432 ± 15 Ma	452 ± 12 Ma	446 ± 12Ma
Devonian		380 ± 6 Ma	401 ± 20 Ma; 367 ± 13 Ma	375 ± 10 Ma	

5.1. Significance of Proterozoic—Cambrian Signatures

The U-Pb zircon ages in low- to middle-grade metamorphic rocks from the CPT (Table 2) preserve memory of previous events owing to the low-temperature metamorphism (i.e., $T < 680$ °C) to which they were subjected, where the zircon isotopic system usually remains closed. In fact, inherited and detrital zircon ages from intermediate to upper crustal levels show age peaks of 2686 ± 34 Ma and 1909 ± 45 Ma (Table 2), and an exceptional very old age of 3242 ± 13 Ma [55], which are missing in high-grade basement rocks (Figure 5) from the CPT, owing to the high-temperature Variscan metamorphism.

Neo-archean (from 2686 ± 34 Ma to 2506 ± 43 Ma), Paleo-proterozoic (from 2455 ± 40 Ma to 1637 ± 49 Ma), Meso-proterozoic (from 1573 ± 42 Ma to 1005 ± 26 Ma), and Neo-proterozoic (from 992 ± 26 Ma to 622 ± 17 Ma) ages represent inheritances (Figure 8a and Table 2) from ancient basements recognizable in the African Craton that collected the remnants of the pan-African orogen, forming the Gondwana supercontinent. The age peaks between 2686 ± 34 Ma and 1573 ± 42 Ma are connected to west-Gondwana domains (Table 2 and Figures 3–8a), whereas the ubiquitous occurrence of zircon ages between 1025 ± 18 Ma and 945 ± 13 Ma (Table 2 and Figures 3–8a) constraints potential source

regions connected to east-Gondwana domains, which are similar to those present in the early Palaeozoic cover sequence of the Saharan Metacraton [55,65,83].

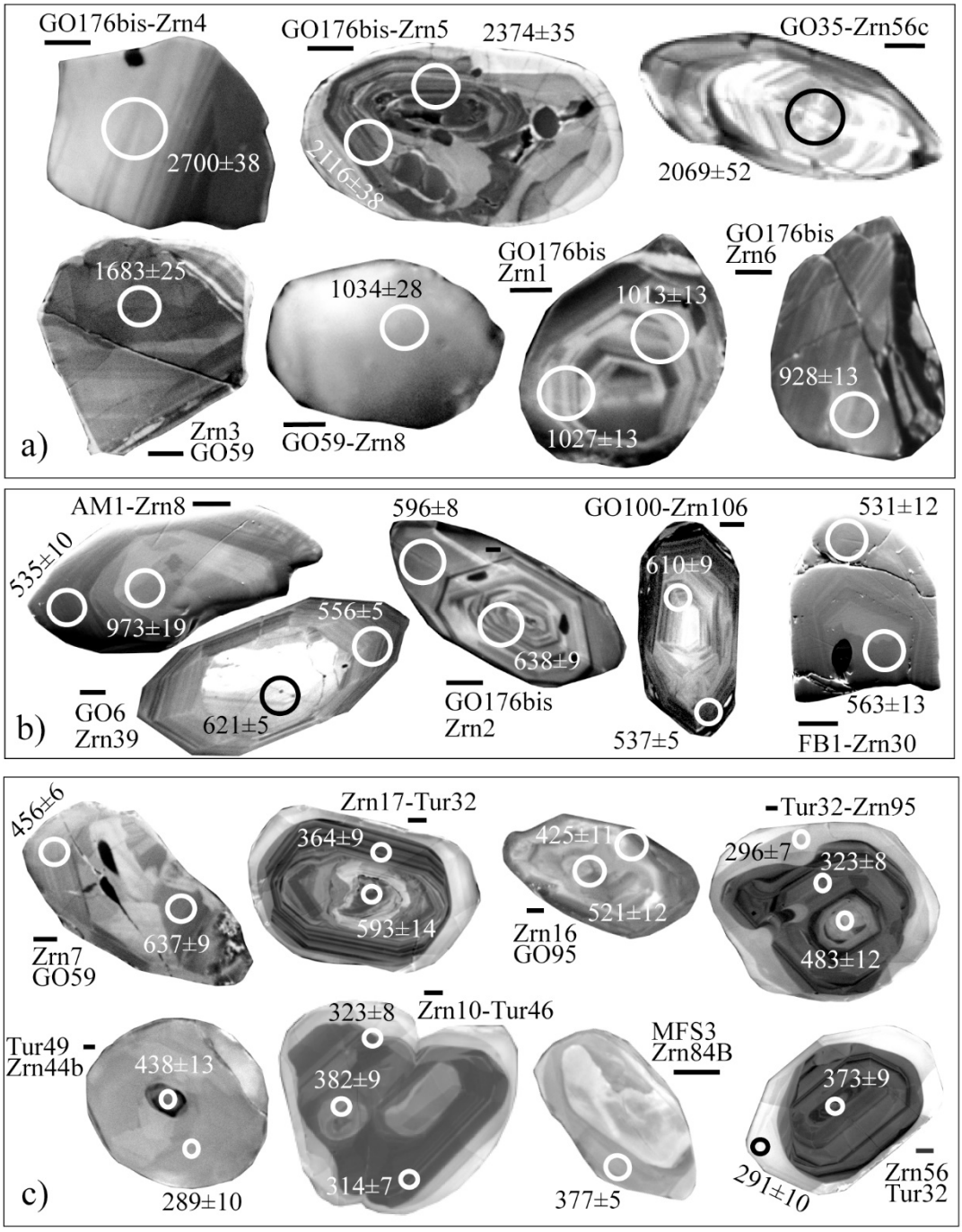

Figure 8. CL and VPSE zircon images grouped from the older to the younger ages (data from [65,66], new U-Pb data and original images for GO176bis, GO59, AM1, FB1 samples). (**a**) Dated zircons showing the clusters from about 2700 Ma to about 928 Ma. (**b**) Dated zircons showing the clusters from about 638 Ma to about 531 Ma; original image for GO100-Zrn106. (**c**) Dated zircons showing ages at about 637 Ma with Ordovician overgrowths (GO59-Zrn7) and Ordovician cores with Carboniferous overgrowths (Tur46-Zrn44b, Tur32-Zrn95); Devonian relict zircons with Carboniferous rim are also shown (Zrn10-Tur46, Zrn56-Tur32). Symbols as in Figure 3.

A more detailed interpretation regards the age peaks between about 649 and 596 Ma, which are present in metasediments of all the considered sectors (Figures 3–6). They could indicate the maximum sedimentation age of the protoliths of the metasediments [65], since they were collected on inherited detrital zircons. This interpretation is coherent with the textural features of the dated

zircons in the metasediments from the Castagna Unit (Figure 3). In fact, some rounded zircon cores in paragneisses, dated at 638 ± 9 Ma and 637 ± 9 Ma, show younger metamorphic overgrowths (Figure 8b GO176 bis Zrn2, Figure 8c; GO59 Zrn7), recording a successive metamorphic history at 596–556 Ma (Figure 8b, e.g., GO6-Zrn39, GO176bis-Zrn2). The orthogneisses hosted by metasediments in which they were intruded at 543–545 Ma [61,66], were affected by a later zircon recrystallization at around 531–527 Ma (Figure 8b, e.g., FB1-Zrn30, Figure 9, e.g., ADR5-Zrn60ar and ADR18-Zrn56) up to about 518 ± 11 Ma (Figure 3b). Accordingly, the metasediments of the Castagna Unit were intruded by Ediacaran granitoids (later metamorphosed during Variscan orogeny), supporting for an age of sedimentation older than 543–545 Ma [61,66], probably around 637 Ma (Figures 3 and 8, and Table 2). Following this interpretation, the few zircon rims dated between 596 and 556 Ma could suitably represent post-depositional metamorphic events. A successive common geological history of metasediments and Ediacaran granitoid intrusions was recorded by zircon overgrowths in these rock types (Figure 8b, e.g., GO176bis-Zrn2, AM1-Zrn8 and FB1-Zrn30), as shown by the age peaks at 519 ± 12 Ma in metasediments (Figure 3a) and at 518 ± 11 Ma in orthogneisses (Figure 3b).

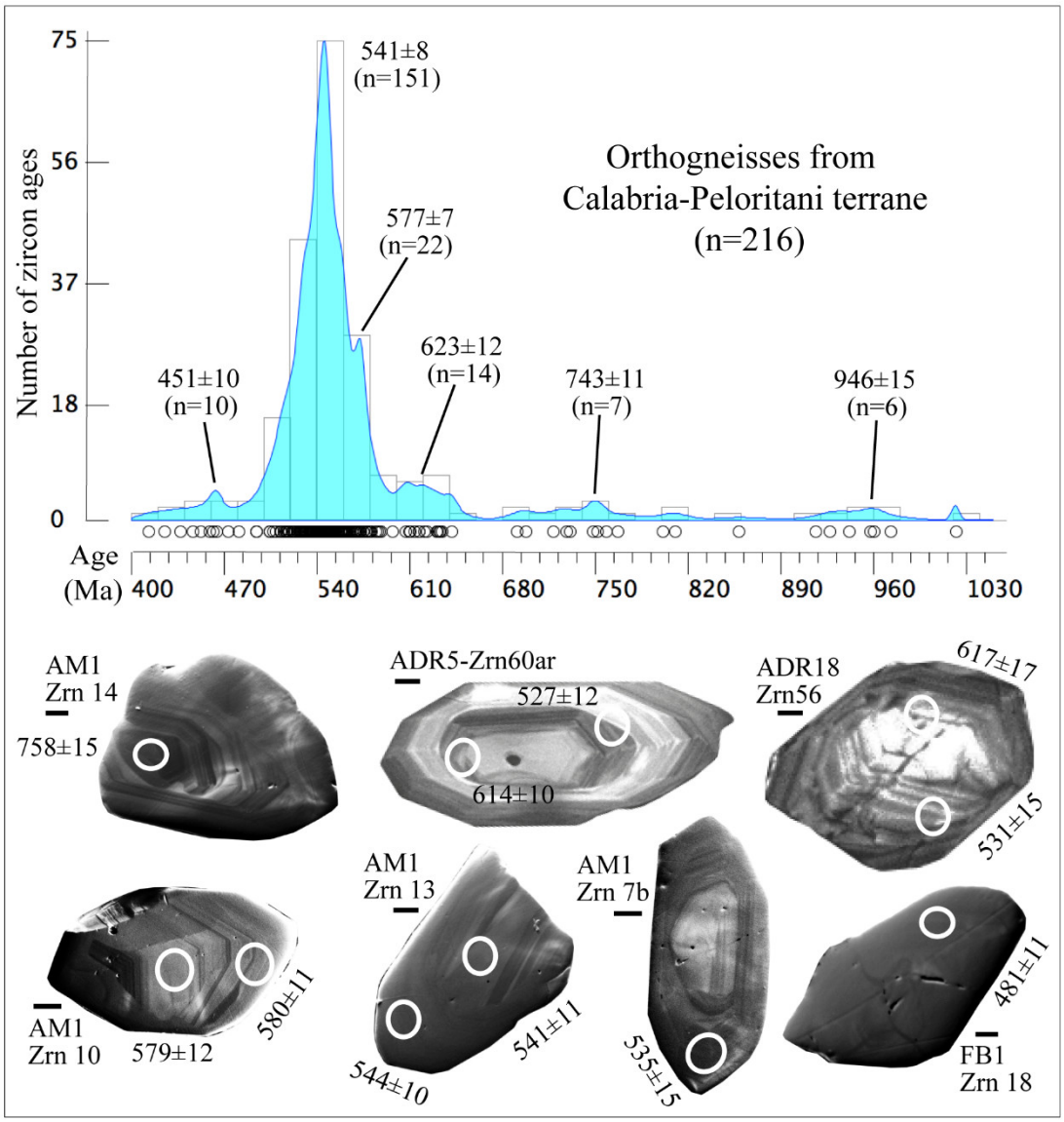

Figure 9. Histogram and probability density plot of U-Pb zircon ages from orthogneisses of Castagna and Sila–Serre units (data by [66], new data from AM1 and FB1 samples), and Aspromonte–Peloritani Unit (data from [55,61]). Spot ages in the selected zircons (CL and VPSE images) replicate the age clusters; note the younger mimetic metamorphic overgrowths on older relict zircons as in ADR18-Zrn56 and AM1-Zrn7b. Symbols as in Figure 3.

As regards the metasediments of the Mandatoriccio Unit [72], the most pronounced age peak occurs at around 622 Ma (Figure 6). However, perturbed and recrystallized zircons dated around 524 Ma and 446 Ma (Figure 6) suggest a replacement of zircon textures due to a fluid activity [7], as evidenced by the network of luminescent veins affecting the crystals (Figure 6, e.g., Zrn28A), probably related to post-depositional metamorphic events. Hence, we interpret the age peak at around 622 Ma as representative of the maximum sedimentation age of the protoliths, similar to the sedimentation age of the Castagna Unit metasediments (Table 2).

Similar interpretation can be also suggested for the metasediments from the Aspromonte–Peloritani Unit. The age peaks at 631 ± 7 Ma from these rocks are numerous, as well as the age peak at 541 ± 6 Ma (Figure 4). According to [61,84], these younger ages (around 541 Ma) represent an event of fast sedimentation and metamorphism up to anatexis. However, this interpretation does not take into account the age signature of 631 ± 7 Ma (Figure 4 and Table 2). Considering the zircon ages that we measured from an amphibolite interbedded with paragneisses of a similar portion of the same unit cropping out in the Aspromonte Massif (sample AS53 and AS53bis), few ages between 565 Ma and 503 Ma are recorded, even into a single crystal (Figure 4, e.g., Zrn71). This wide range of ages suggests a U-Pb isotopic system opening, which supports a different interpretation. We interpret the age peak of zircons at 541 ± 6 Ma (Figure 4, Table 2), in the paragneisses of the Aspromonte–Peloritani Unit, as related to a fluid-assisted metamorphism. In addition, since also these paragneisses were intruded by the Ediacaran granitoids (dated around 545 Ma [55,61]), the sedimentation of their protoliths was likely at around 631 Ma (Figure 4), with the later fluid-assisted metamorphism (at around 541 Ma) likely connected to the emplacement of the granitoids.

Moreover, this interpretation is strongly supported by the similar sedimentation age of the protoliths of the Castagna Unit paragneisses (cf. Table 2).

Considering the U-Pb zircon ages in high-grade metasediments and metabasites belonging to the Sila–Serre Unit, as well as those in a garnet-biotite gneiss derived from a sliver of Alpine tectonic melange at the Calabria–Lucania boundary (Figure 5), the distribution of pre-Carboniferous zircon ages in these rocks is complex for the relevant Variscan metamorphic imprint. A few ages in metasediments are around 1784 Ma, 992 Ma, 714 Ma, 649 Ma, and 596 Ma (Figure 5 and Table 2); whereas a higher frequency of ages around 556 Ma, 452 Ma, and 375 Ma are shown in Figure 5. However, even these metasediments were intruded by Ediacaran granitoids and gabbros dated at around 543 Ma and 579 Ma, respectively [17,65,69]. Hence, the age peaks around 556–509 Ma can be related to Ediacaran magmatism that triggered a metamorphic recrystallization opening the U-Pb system of zircon [65]. According to this interpretation, the sedimentation age of high-grade metasediments from the CPT was older than 556 Ma, presumably between 596 and 649 Ma (Table 2), as shown by an inherited zircon age from the orthogneiss interbedded with the high-grade metasediments dated at around 610 Ma with an overgrowth around 537 Ma (Figure 8b, e.g., GO100 Zrn106). Therefore, geochronological and geological aspects suggest that even the protoliths of high-grade metasediments from the CPT were formed in Neo-proterozoic and were later affected by Ediacaran magmatism and metamorphism [65].

5.2. Significance of Ordovician—Silurian Signatures

A characteristic large cluster of Ordovician–Silurian ages has been revealed on zircons from paragneisses of the Mandatoriccio Paragneiss Unit (446 ± 12 Ma) and the lower continental crust (452 ± 12 Ma) of the Sila–Serre Unit, and from metasediments of the Castagna Unit (452 ± 10 Ma) (Table 2). The Ordovician ages of zircons from Castagna and Sila–Serre units were detected both at the core of grains showing Variscan overgrowths (Figure 8c, e.g., Tur 32 Zrn95, Tur 49 Zrn 44b) and at rims of Cambrian zircons as well (Figure 3, e.g., GO59 Zrn4b). These Ordovician–Silurian ages represent an important thermal-metamorphic event in these units, that, however, did not involve the Aspromonte–Peloritani Unit, due to the lack of age peak at around 450 Ma (Figure 4 and Table 2). In contrast, the Lower Complex contains Ordovician–Silurian volcanic rocks (Table 2) emplaced synchronously with the deposition of the protoliths of phyllites and meta-limestones, with the volcanic rocks metamorphosed as porphyroids and metandesites during the Variscan orogeny [62].

5.3. Significance of Devonian Signatures

A few clusters of Devonian ages at around 380 Ma and 375 Ma were obtained in the Sila–Serre Unit (Figure 8c, e.g., Tur 32 Zrn56, MFS3 Zrn84B, Tur46 Zrn10) and in amphibolite from the Aspromonte–Peloritani Unit (Figure 4, e.g., AS53bis Zrn3; Table 2), respectively, which suggest Eo-Variscan precursor events, as revealed in other crystalline basements of the southern European Variscan belt [85].

5.4. From Pre-Variscan to Variscan Geodynamic Frameworks Revealed by Zircon Ages

In the puzzle of pre-Carboniferous geological events recorded in the CPT, the Ediacaran magmatism played a pivoting role, producing the protoliths of the orthogneiss that intruded the metasediments of the Castagna, Aspromonte–Peloritani, and Sila–Serre units, which are dated at around 545 and 543 Ma [55,61,66]. A relevant peak at 623 ± 12 Ma emerges from the age spectrum in the orthogneisses from Calabria (Figure 9). The protoliths of the orthogneisses are derived from mixing of mantle and crustal magmas [86], as they record a crustal signature, with inherited zircons patterns similar to the detrital zircon pattern from the metasediments in which they intruded. In fact, the relict age of 614 ± 10 Ma (Figure 9, e.g., ADR5 Zrn60ar) in orthogneisses nearly coincides with the possible sedimentation age of the metasedimentary protoliths of the Castagna Unit (637 ± 9 Ma), the Aspromonte–Peloritani Unit (631 ± 7 Ma), and the Sila–Serre Unit (596–649 Ma). In addition, a mafic Ediacaran magmatism (around 579 Ma) was also reported at the base of the deep crust sector of the Sila–Serre Unit [65].

Accordingly, the following scenario can be reconstructed: a peri-Gondwana metamorphic basement, formed by the Aspromonte–Peloritani Unit, the Castagna Unit, and the Mandatoriccio Unit and the lower crustal level of the Sila–Serre Unit, was formerly involved in Pan-African orogeny, thus representing a Cadomian fragment. The age clusters between 596 and 649 Ma can be interpreted as the sedimentation ages of the protoliths of the metasediments of these units, which were successively affected by metamorphic events around 556–509 Ma (Table 2), connected to acidic and mafic Ediacaran magmatism.

Successively, the Palaeozoic protoliths of the low-grade phyllite units (i.e., the Lower Complex, the Stilo Unit, the Bocchigliero Phyllite, and Stilo-Pazzano Phyllite units, within the Sila-Serre Unit), together with Ordovician–Silurian volcanic to subvolcanic rocks [48–51], may have started infilling a basin controlled by extensional tectonics, which affected the northern Gondwana margin during the Middle Ordovician incipient phases of the Rheic rifting [87,88] (Figure 10a). Throughout this extensional event, fluid-assisted metamorphism may have been favored, as observed for similar tectonic contexts [89,90], determining perturbed textures in zircons (dated around 450 Ma) from the Castagna Unit, as well as from the Mandatoriccio Unit and the lower crustal level of the Sila–Serre Unit [65], all forming part of the Gondwana bedrock of the Palaeozoic covers (Figure 10a).

The deposition of the protoliths of the low-grade phyllite units carried on during Early Devonian, when the beginning of a further dismembering of the northern Gondwana, related to the Palaeotethys rifting, occurred [91]. Therefore, the deposition of the low-grade phyllite units protoliths protracted at least up to Upper Devonian [48–51] in the Palaeotethys basin, as part of the sedimentary level of the upper oceanic crust, and along the passive margin of Gondwana (Figure 10b).

According to [45], the CPT took part in the growth of the southern Variscan belt, due to the subduction of the Palaeotethys–Gondwana beneath Laurussia [91–96]. The Variscan zircon U-Pb ages from the CPT indicate that the subduction occurred up to the Upper Mississippian–Lower Pennsylvanian, as also recorded in metamorphic terranes from other sectors of the southern Variscan belt like Sardinia [97,98]. In this broader subduction context, the Gondwana terranes, included in the Mandatoriccio Unit and the lower continental crust of Sila–Serre Unit, Castagna Unit, Aspromonte–Peloritani Unit (and likely in the Fiume Pomo Unit, Mandanici Unit, and Mammola Paragneiss Unit) (Figure 2) along with the Palaeozoic covers, included in the Lower Complex, Stilo Unit, and Bocchigliero Phyllite and Stilo-Pazzano Phyllite units of the Sila–Serre Unit (Figure 2), were involved in the accretion of the southern Variscan belt. More in detail, the Palaeozoic sediments were scraped off mostly along the front of the southern Variscan belt, whereas the Gondwana terranes (as well as

part of the Paleozoic covers) were under-thrusted at depth, and subjected to greenschists-, amphibolite-, and granulite-facies metamorphic conditions (Figure 10c).

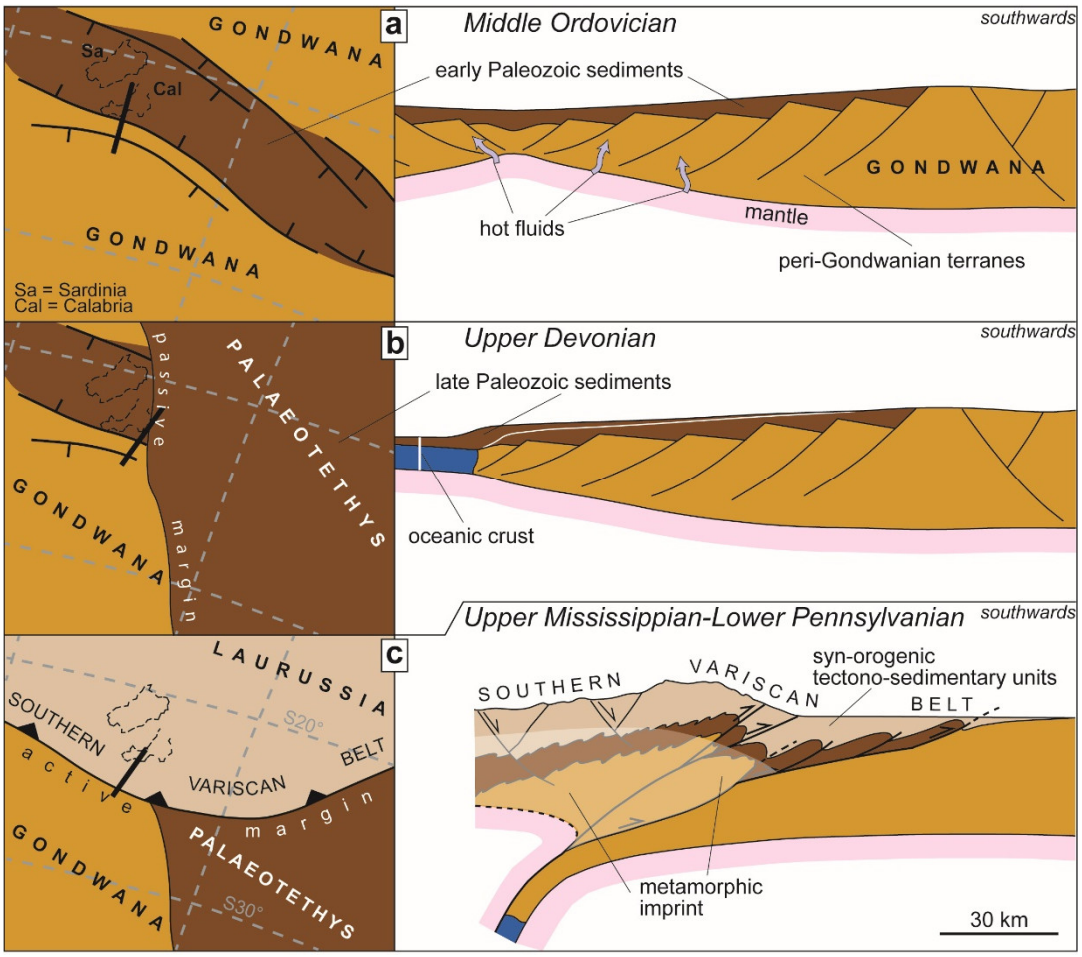

Figure 10. Plan view (left column) and in cross section (right column) geodynamic reconstruction of the northern Gondwana sector, framed in the (**a**) Middle Ordovician, following extensional tectonics related to incipient Rheic rifting (plan view, modified from [87]); (**b**) Upper Devonian, following the opening of the Palaeotethys (plan view, modified from [91]); (**c**) Upper Mississippian–Lower Pennsylvanian, following the subduction of the Palaeotethys–Gondwana beneath Laurussia, that formed the Southern Variscan Belt (plan view, modified from [96]; cross section, modified from [45]); the area of the belt subjected to Variscan metamorphic imprint is indicated with transparency. In the plan view geodynamic reconstructions the possible location of the CPT, as well as of the Sardina, is indicated; the thick black segment represents the trace of the cross section; meridians and parallel spacing is of 10° (roughly adapted after [96]).

6. Conclusions

The present review of U-Pb zircon ages collected in different crustal domains of the CPT allowed us to constrain the timing of sedimentation, tectonic, metamorphic, and magmatic events that affected this key sector of the Southern Variscan Belt from Precambrian to Permian. This was possible since several crustal levels stored in the CPT preserve memory of Pan-African orogeny derived from the break-up of peri-Gondwana terranes and Ordovician-Silurian magmatic and sedimentation events. All these domains were later affected by metamorphism and magmatism during Variscan orogeny. A revisiting of the timing of the events revealed by comparing the internal zircon textures and the related U-Pb age clusters, highlights the following scenario:

- The age peaks from around 2500 Ma to 1600 Ma and 1000 Ma in the deep–intermediate crustal levels testify that the origin of the CPT was related to fragments of West and East Gondwana realms, respectively.
- The sedimentation age of the considered Cadomian terrane (i.e., the CPT), was around 630 Ma; this terrane was later affected by Ediacaran (579–540 Ma) bimodal (i.e., gabbros and granitoids) intrusions, which induced zircon recrystallization in host metasediments as shown by overgrowths dated 556–509 Ma.
- An Ordovician–Silurian extensional tectonic phase (at around 450 Ma) connected to the incipient opening, northwards, of the Rheic ocean, affected the northern Cadomian terranes inducing fluid-assisted metamorphism in some domains. At the same time on this Cadomian substrate, sedimentation and volcanic to subvolcanic activity took place, forming the protoliths of the future Variscan upper crust.
- Subduction of the Palaeotethys–Gondwana margin beneath Laurussia began around 347 Ma with under-thrusting of the formerly Gondwana substrate, and induced middle- to high-grade metamorphism in this crust. The Ordovician–Silurian sedimentary cover was scraped off along the front of the Southern Variscan Belt and subjected to low-grade metamorphism. After the compressive tectonic phase, decompression of the whole orogenic system occurred around 320 Ma and led to uplifting of the chain with emplacement of huge granitic intrusions and partial melting of the fertile rocks within the deeper crust. The last metamorphic and magmatic stages occurred around 280 Ma, when the southern Variscan orogenic cycle ended.

Supplementary Materials: The following are available online at www.mdpi.com/2075-163X/10/11/944/s1, Table S1: LA-ICP-MS zircon U-Pb age data from AM1, FB1, AS53, AS53bis, GO176bis, GO59 samples. Appendix S1: Analytical methods. (The reference 99 is cited in the Supplementary Materials)

Author Contributions: Conceptualization, all authors; methodology, all authors; data curation, F.M., V.F.; writing—original draft preparation, all authors; writing—review and editing, all authors; All authors have read and agreed to the published version of the manuscript.

Funding: This research was funded by University of Bari (Italy), grant n. 00596609 ricat 01.

Acknowledgments: We thank A. Langone for his assistance during the instrumental analyses. We are grateful to two anonymous reviewers for their constructive comments.

Conflicts of Interest: The authors declare no conflict of interest. The funders had no role in the design of the study, in the collection, analyses, or interpretation of data; in the writing of the manuscript, or in the decision to publish the results.

References

1. Hoskin, P.W.O.; Schaltegger, U. The composition of zircon and igneous and metamorphic petrogenesis. *Zircon* **2018**, *53*, 27–62.
2. Corfu, F.; Hanchar, J.M.; Hoskin, P.W.O.; Kinny, P. Atlas of zircon textures. *Zircon* **2003**, *53*, 469–500.
3. Nasdala, L.; Zhang, M.; Kempe, U.; Panczer, G.; Gaft, M.; Andrut, M.; Plötze, M. Spectroscopic methods applied to zircon. *Zircon* **2003**, *53*, 427–467, doi:10.1515/9781501509322-018.
4. Griffin, B.; Michael, J.; Joy, D. A Comparison of a Luminescence-based VPSE and an Electron-based GSED for SE and CL Imaging in Variable Pressure SEM with Conventional SE imaging. *Microsc. Microanal.* **2010**, *16*, doi:10.1017/s1431927610058691.
5. Gehrels, G. Detrital zircon U-Pb geochronology applied to tectonics. *Annu. Rev. Earth Planet. Sci.* **2014**, *42*, 127–149.
6. Rubatto, D.; Hermann, J. Experimental zircon/melt and zircon/garnet trace element partitioning and implications for the geochronology of crustal rocks. *Chem. Geol.* **2007**, *241*, doi:10.1016/j.chemgeo.2007.01.027.
7. Rubatto, D. Zircon: The Metamorphic Mineral. *Rev. Mineral. Geochem.* **2017**, *83*, 261–295, doi:10.2138/rmg.2017.83.09.
8. Fornelli, A.; Langone, A.; Micheletti, F.; Piccarreta, G. Time and duration of Variscan high-temperature metamorphic processes in the south European Variscides: Constraints from U-Pb chronology and trace

element chemistry of zircon. *Mineral. Petrol.* **2011**, *103*, 101–122, doi:10.1007/s00710-011-0156-8.
9. Xia, Q.X.; Zheng, Y.F.; Yuan, H.; Wu, F.Y. Contrasting Lu-Hf and U-Th-Pb isotope systematics between metamorphic growth and recrystallization of zircon from eclogite-facies metagranites in the Dabie orogen, China. *Lithos* **2009**, *112*, 477–496, doi:10.1016/j.lithos.2009.04.015.
10. Fornelli, A.; Langone, A.; Micheletti, F.; Piccarreta, G. REE partition among zircon, orthopyroxene, amphibole and garnet in a high-grade metabasic system. *Geol. Mag.* **2018**, *155*, doi:10.1017/S001675681700067X.
11. Yakymchuk, C.; Clark, C.; White, R.W. Phase Relations, Reaction Sequences and Petrochronology. *Rev. Mineral. Geochem.* **2017**, *83*, 13–53, doi:10.2138/rmg.2017.83.2.
12. Buick, I.S.; Clark, C.; Rubatto, D.; Hermann, J.; Pandit, M.; Hand, M. Constraints on the Proterozoic evolution of the Aravalli-Delhi Orogenic belt (NW India) from monazite geochronology and mineral trace element geochemistry. *Lithos* **2010**, *120*, 511–528, doi:10.1016/j.lithos.2010.09.011.
13. Whitehouse, M.J.; Platt, J.P. Dating high-grade metamorphism - Constraints from rare-earth elements in zircon and garnet. *Contrib. Mineral. Petrol.* **2003**, *145*, doi:10.1007/s00410-002-0432-z.
14. Schaltegger, U.; Davies, J.H.F.L. Petrochronology of Zircon and Baddeleyite in Igneous Rocks: Reconstructing Magmatic Processes at High Temporal Resolution. *Rev. Mineral. Geochem.* **2017**, *83*, 297–328, doi:10.2138/rmg.2017.83.10.
15. Zhou, L.G.; Xia, Q.X.; Zheng, Y.F.; Chen, R.X. Multistage growth of garnet in ultrahigh-pressure eclogite during continental collision in the Dabie orogen: Constrained by trace elements and U-Pb ages. *Lithos* **2011**, *127*, 101–127, doi:10.1016/j.lithos.2011.08.010.
16. Zhang, S.B.; Zheng, Y.F.; Zhao, Z.F. Temperature effect over garnet effect on uptake of trace elements in zircon of TTG-like rocks. *Chem. Geol.* **2010**, *274*, 108–125, doi:10.1016/j.chemgeo.2010.04.002.
17. Micheletti, F.; Fornelli, A.; Piccarreta, G.; Tiepolo, M. U-Pb zircon data of Variscan meta-igneous and igneous acidic rocks from an Alpine shear zone in Calabria (southern Italy). *Int. J. Earth Sci.* **2011**, *100*, 139–155, doi:10.1007/s00531-009-0497-2.
18. Malusà, M.G.; Garzanti, E. The Sedimentology of Detrital Thermochronology. In *Fission-Track Thermochronology and Its Application to Geology*; Springer: Cham, Switzerland, 2019; pp. 123–143.
19. Mattioli, M.; Lustrino, M.; Ronca, S.; Bianchini, G. Alpine subduction imprint in Apennine volcaniclastic rocks. Geochemical-petrographic constraints and geodynamic implications from Early Oligocene Aveto-Petrignacola Formation (N Italy). *Lithos* **2012**, *134–135*, 201–220, doi:10.1016/j.lithos.2011.12.017.
20. Lu, G.; Di Capua, A.; Winkler, W.; Rahn, M.; Guillong, M.; von Quadt, A.; Willett, S.D. Restoring the source-to-sink relationships in the Paleogene foreland basins in the Central and Southern Alps (Switzerland, Italy, France): A detrital zircon study approach. *Int. J. Earth Sci.* **2019**, *108*, 1817–1834, doi:10.1007/s00531-019-01734-6.
21. Fornelli, A.; Gallicchio, S.; Micheletti, F.; Langone, A. Preliminary U-Pb Detrital Zircon Ages from Tufiti di Tusa Formation (Lucanian Apennines, Southern Italy): Evidence of Rupelian Volcaniclastic Supply. *Minerals* **2020**, 1–24, doi:10.3390/min10090786.
22. Fornelli, A.; Micheletti, F.; Langone, A.; Perrone, V. First U-Pb detrital zircon ages from Numidian sandstones in Southern Apennines (Italy): Evidences of African provenance. *Sediment. Geol.* **2015**, *320*, doi:10.1016/j.sedgeo.2015.02.005.
23. Amodio-Morelli, L.; Bonardi, G.; Colonna, V.; Dietrich, D.; Giunta, G.; Ippolito, F.; Liguori, V.; Lorenzoni, S.; Paglionico, A.; Perrone, V.; et al. L'Arco Calabro-Peloritano nell'Orogene Appenninico-Maghrebide. *Mem. della Soc. Geol. Ital.* **1976**, *17*, 1–60.
24. Bonardi, G.; Cavazza, W.; Perrone, V.; Rossi, S. Calabria-Peloritani terrane and northern Ionian Sea. In *Anatomy of an Orogen: The Apennines and Adjacent Mediterranean Basins*; Springer: Dutch, The Netherlands, 2001; pp. 287–306.
25. Schenk, V. U-Pb and Rb-Sr radiometric dates and their correlation with metamorphic events in the granulite-facies basement of the serre, Southern Calabria (Italy). *Contrib. Mineral. Petrol.* **1980**, *73*, 23–38, doi:10.1007/BF00376258.
26. Piccarreta, G. Deep-rooted overthrusting and blueschistic metamorphism in compressive continental margins. An example from Calabria (Southern Italy). *Geol. Mag.* **1981**, *118*, 539–544, doi:10.1017/S0016756800032908.
27. Rossetti, F.; Faccenna, C.; Goffé, B.; Monié, P.; Argentieri, A.; Funiciello, R.; Mattei, M. Alpine structural and metamorphic signature of the Sila Piccola Massif nappe stack (Calabria, Italy): Insights for the tectonic

evolution of the Calabrian Arc. *Tectonics* **2001**, *20*, 112–133.
28. Langone, A.; Gueguen, E.; Prosser, G.; Caggianelli, A.; Rottura, A. The Curinga-Girifalco fault zone (northern Serre, Calabria) and its significance within the Alpine tectonic evolution of the western Mediterranean. *J. Geodyn.* **2006**, *42*, 140–158, doi:10.1016/j.jog.2006.06.004.
29. Pezzino, A.; Angi, G.; Fazio, E.; Fiannacca, P.; Lo Giudice, A.; Ortolano, G.; Punturo, R.; Cirrincione, R.; de Vuono, E. Alpine metamorphism in the aspromonte massif: Implications for a new framework for the southern sector of the Calabria-Peloritani Orogen, Italy. *Int. Geol. Rev.* **2008**, *50*, 423–441, doi:10.2747/0020-6814.50.5.423.
30. Heymes, T.; Monié, P.; Arnaud, N.; Pêcher, A.; Bouillin, J.P.; Compagnoni, R. Alpine tectonics in the Calabrian-Peloritan belt (southern Italy): New 40Ar/39Ar data in the Aspromonte Massif area. *Lithos* **2010**, *114*, 451–472, doi:10.1016/j.lithos.2009.10.011.
31. Ortolano, G.; Visalli, R.; Fazio, E.; Fiannacca, P.; Godard, G.; Pezzino, A.; Punturo, R.; Sacco, V.; Cirrincione, R. Tectono-metamorphic evolution of the Calabria continental lower crust: The case of the Sila Piccola Massif. *Int. J. Earth Sci.* **2020**, 1–25, doi:10.1007/s00531-020-01873-1.
32. Brandt, S.; Schenk, V. Metamorphic response to Alpine thrusting of a crustal-scale basement nappe in southern Calabria (Italy). *J. Petrol.* **2020**, doi:10.1093/petrology/egaa063.
33. Festa, V.; Cicala, M.; Tursi, F. The Curinga—Girifalco Line in the framework of the tectonic evolution of the remnant Alpine chain in Calabria (southern Italy). *Int. J. Earth Sci.* **2020**, doi:10.1007/s00531-020-01918-5.
34. Tursi, F.; Bianco, C.; Brogi, A.; Caggianelli, A.; Prosser, G.; Ruggieri, G.; Braschi, E. Cold subduction zone in northern Calabria (Italy) revealed by lawsonite–clinopyroxene blueschists. *J. Metamorph. Geol.* **2020**, *38*, 451–469, doi:10.1111/jmg.12528.
35. Festa, V.; Messina, A.; Paglionico, A.; Piccarreta, G.; Rottura, A. Pre-Triassic history recorded in the Calabria-Peloritani segment of the Alpine chain, southern Italy. An overview. *Period. Mineral.* **2004**, *73*, 57–71.
36. Dubois, R. Définition d'un socle antéhercynien en Calabre. *Comptes rendus l'Académie Sci. Paris* **1971**, *272*, 2052–2055.
37. Caggianelli, A.; Prosser, G.; Rottura, A. Thermal history vs. fabric anisotropy in granitoids emplaced at different crustal levels: An example from Calabria, Southern Italy. *Terra Nova* **2000**, *12*, 109–116, doi:10.1111/j.1365-3121.2000.00280.x.
38. Colonna, V.; Lorenzoni, S.; Zanettin Lorenzoni, E. Sull'esistenza di due complessi metamorfici lungo il bordo sud-orientale del massiccio "granitico" delle Serre (Calabria). *Boll. della Soc. Geol. Ital.* **1973**, *92*, 801–830.
39. Borghi, A.; Colonna, V.; Compagnoni, R. Structural and metamorphic evolution of the Bocchigliero and Mandatoriccio complexes in the Sila nappe (Calabrian-Peloritan Arc, Southern Italy). In *The Contributions to the Geology of Italy with Special Regards to the Palaeozoic Basements*; Carmignani, L., Sassi, F.P., Eds.; IGCP Newsletter: Siena, Italy, 1992; Volume 276, pp. 321–334.
40. Festa, V.; Caggianelli, A.; Kruhl, J.H.; Liotta, D.; Prosser, G.; Gueguen, E.; Paglionico, A. Late-Hercynian shearing during crystallization of granitoid magmas (Sila massif, southern Italy): Regional implications. *Geodin. Acta* **2006**, *19*, 185–195, doi:10.3166/ga.19.185-195.
41. Langone, A.; Godard, G.; Prosser, G.; Caggianelli, A.; Rottura, A.; Tiepolo, M. P-T-t path of the Hercynian low-pressure rocks from the Mandatoriccio complex (Sila massif, Calabria, Italy): New insights for crustal evolution. *J. Metamorph. Geol.* **2010**, *28*, 137–162, doi:10.1111/j.1525-1314.2009.00858.x.
42. Langone, A.; Caggianelli, A.; Festa, V.; Prosser, G. Time Constraints on the Building of the Serre Batholith: Consequences for the Thermal Evolution of the Hercynian Continental Crust Exposed in Calabria (Southern Italy). *J. Geol.* **2014**, *122*, 183–199, doi:10.1086/675227.
43. Festa, V.; Caggianelli, A.; Langone, A.; Prosser, G. Time–space relationships among structural and metamorphic aureoles related to granite emplacement: A case study from the Serre Massif (southern Italy). *Geol. Mag.* **2013**, *150*, 441–454, doi:10.1017/S0016756812000714.
44. Festa, V.; Tursi, F.; Caggianelli, A.; Spiess, R. The tectono-magmatic setting of the Hercynian upper continental crust exposed in Calabria (Italy) as revealed by the 1:10,000 structural-geological map of the Levadio stream area. *Ital. J. Geosci.* **2018**, *137*, 165–174, doi:10.3301/IJG.2018.03.
45. Tursi, F.; Spiess, R.; Festa, V.; Fregola, R.A. Hercynian subduction-related processes within the metamorphic continental crust in Calabria (southern Italy). *J. Metamorph. Geol.* **2020**, *38*, 771–793, doi:10.1111/jmg.12537.

46. Angì, G.; Cirrincione, R.; Fazio, E.; Fiannacca, P.; Ortolano, G.; Pezzino, A. Metamorphic evolution of preserved Hercynian crustal section in the Serre Massif (Calabria–Peloritani Orogen, southern Italy). *Lithos* **2010**, *115*, 237–262, doi:10.1016/j.lithos.2009.12.008.
47. Acquafredda, P.; Barbieri, M.; Lorenzoni, S.; Trudu, C.; Zanettin-Lorenzoni, E. Metamorphism of the Mandatoriccio Unit in the context of the Hercynian and pre-Hercynian evolution of the Calabrian-Peloritani Arc (Southern Italy). *Rend. Lincei* **1992**, *3*, 151–161.
48. Bouillin, J.P.; Majestè-Menjoulas, C.; Baudelot, S.; Cygan, C.; Fournier-Vinas, C.H. Les formations paleozoiques de l'Arc Calabro-Peloritain dans leur cadre structural. *Boll. della Soc. Geol. Ital.* **1987**, *106*, 683–698.
49. Acquafredda, P.; Lorenzoni, S.; Zanettin-Lorenzoni, E. La sequenza Paleozoica dell'Unità di Bocchigliero (Sila, Calabria). *Rend. della Soc. Geol. Ital.* **1988**, *11*, 5–22.
50. Acquafredda, P.; Lorenzoni, S.; Zanettin Lorenzoni, E. Paleozoic sequences and evolution of the Calabrian Peloritani Arc (Southern Italy). *Terra Nova* **1994**, *6*, 582–594.
51. Navas-Parejo, P.; Rodríguez-Cañero, R.; Martín-Algarra, A.; Somma, R.; Perrone, V. Conodont-based stratigraphy in the Devonian of the Serre Massif (Southern Italy). *Stratigraphy* **2015**, *12*, 1–21.
52. Acquafredda, P.; Lorenzoni, S.; Zanettin Lorenzoni, E.; Barbieri, M.; Trudu, C. The age of volcanism and metamorphism of the Bocchigliero Paleozoic sequence (Sila—Southern Italy). *Rend. Lincei* **1991**, *2*, 145–156, doi:10.1007/BF03001418.
53. Colonna, V.; Piccarreta, G. Schema strutturale della Sila Piccola. *Boll. della Soc. Geol. Ital.* **1975**, *94*, 3–16.
54. Paglionico, A.; Piccarreta, G. Le Unità del Fiume Pomo e di Castagna nelle Serre settentrionali (Calabria). *Boll. Della Soc. Geol. Ital.* **1976**, *95*, 27–37.
55. Williams, I.S.; Fiannacca, P.; Cirrincione, R.; Pezzino, A. Peri-Gondwanan origin and early geodynamic history of NE Sicily: A zircon tale from the basement of the Peloritani Mountains. *Gondwana Res.* **2012**, *22*, 855–865, doi:10.1016/j.gr.2011.12.007.
56. Cirrincione, R.; Fazio, E.; Fiannacca, P.; Ortolano, G.; Pezzino, A.; Punturo, R. The Calabria-Peloritani Orogen, a composite terrane in Central Mediterranean; Its overall architecture and geodynamic significance for a pre-Alpine scenario around the Tethyan basin. *Period. Mineral.* **2015**, *84*, 701–749, doi:10.2451/2015PM0446.
57. Crisci, G.M.; Donati, G.; Messina, A.; Russo, S.; Perrone, V. L'Unita' Superiore dell'Aspromonte. Studio geologico e petrografico. *Rend. della Soc. Ital. Mineral. Petrol.* **1982**, *38*, 989–1014.
58. Graessner, T.; Schenk, V. Low-pressure metamorphism of Palaeozoic pelites in the Aspromonte, southern Calabria: Constraints for the thermal evolution in the Calabrian crustal cross-section during the Hercynian orogeny. *J. Metamorph. Geol.* **1999**, *17*, 157–172, doi:10.1046/j.1525-1314.1999.00188.x.
59. Bouillin, J.P. Nouvelle interprétation de la liaison Apennin-Maghrébides en Calabre; conséquences sur la paléogéographie téthysienne entre Gibraltar et les Alpes. *Rev. Géol. Dyn. Géogr. Phys.* **1984**, *25*, 321–338.
60. Cirrincione, R.; Fazio, E.; Ortolano, G.; Pezzino, A.; Punturo, R. Fault-related rocks: Deciphering the structural-metamorphic evolution of an accretionary wedge in a collisional belt, NE Sicily. *Int. Geol. Rev.* **2012**, *54*, 940–956, doi:10.1080/00206814.2011.623022.
61. Fiannacca, P.; Williams, I.S.; Cirrincione, R.; Pezzino, A. The augen gneisses of the Peloritani Mountains (NE Sicily): Granitoid magma production during rapid evolution of the northern Gondwana margin at the end of the Precambrian. *Gondwana Res.* **2013**, *23*, 782–796, doi:10.1016/j.gr.2012.05.019.
62. Trombetta, A.; Cirrincione, R.; Corfu, F.; Mazzoleni, P.; Pezzino, A. Mid-Ordovician U-Pb ages of porphyroids in the Peloritan Mountains (NE Sicily): Palaeogeographical implications for the evolution of the Alboran microplate. *J. Geol. Soc.* **2004**, *161*, 265–276, doi:10.1144/0016-764903-068.
63. Cirrincione, R.; Fiannacca, P.; Lo Giudice, A.; Pezzino, A. Evidence of early Palaeozoic continental rifting from mafic metavolcanics of Southern Peloritani Mountains (north-eastern Sicily, Italy). *Ofioliti* **2005**, *30*, 15–25, doi:10.4454/ofioliti.v30i1.237.
64. Somma, R.; Navas-Parejo, P.; Martín-Algarra, A.; Rodríguez-Cañero, R.; Perrone, V.; Martínez-Pérez, C. Paleozoic stratigraphy of the Longi-Taormina Unit (PeloritanianMountains, southern Italy). *Stratigraphy* **2013**, *10*, 127–152.
65. Fornelli, A.; Micheletti, F.; Piccarreta, G. Late-Proterozoic to Paleozoic history of the peri-Gondwana Calabria–Peloritani Terrane inferred from a review of zircon chronology. *SpringerPlus* **2016**, *5*, 1–19, doi:10.1186/s40064-016-1839-8.
66. Micheletti, F.; Barbey, P.; Fornelli, A.; Piccarreta, G.; Deloule, E. Latest precambrian to early cambrian U-

Pb zircon ages of augen gneisses from Calabria (Italy), with inference to the Alboran microplate in the evolution of the peri-Gondwana terranes. *Int. J. Earth Sci.* **2007**, *96*, 843–860, doi:10.1007/s00531-006-0136-0.

67. Fornelli, A.; Piccarreta, G.; Micheletti, F. In situ U-Pb Dating Combined with SEM Imaging on Zircon—An Analytical Bond for Effective Geological Recontructions. In *Geochronol.-Methods Case Stud.*; Nils-Axel Morner, N.-A., Ed.; IntechOpen: London, UK, 2014.
68. Vermeesch, P. On the visualisation of detrital age distributions. *Chem. Geol.* **2012**, *312–313*, 190–194, doi:10.1016/j.chemgeo.2012.04.021.
69. Micheletti, F.; Fornelli, A.; Piccarreta, G.; Barbey, P.; Tiepolo, M. The basement of Calabria (southern Italy) within the context of the Southern European Variscides: LA-ICP-MS and SIMS U-Pb zircon study. *Lithos* **2008**, *104*, 1–11, doi:10.1016/j.lithos.2007.11.003.
70. Laurita, S.; Prosser, G.; Rizzo, G.; Langone, A.; Tiepolo, M.; Laurita, A. Geochronological study of zircons from continental crust rocks in the Frido Unit (southern Apennines). *Int. J. Earth Sci.***2014**, *104*, 179–203, doi:10.1007/s00531-014-1077-7.
71. Langone, A. Metamorfismo Ercinico di Bassa-Pressione: Evoluzione Tettonico-Metamorfica del Complesso di Mandatoriccio (Massiccio della Sila—Calabria). Ph.D Thesis, Alma Mater Studiorum Università di Bologna, Bologna, Italy, 2008.
72. Langone, A. Hercynian low-pressure metamorphism: Tectono-metamorphic evolution of the Mandatoriccio complex (Sila massif—Calabria). *Plinius* **2008**, *34*, 81–89.
73. Langone, A.; Micheletti, F. Provenance of Hercynian medium-low grade metasediments in northern Calabria (southern Italy): Evidence from LA-ICP-MS U-Pb data of detrital zircons from the Mandatoriccio complex. *Rend. Online Soc. Geol. Ital.* **2012**, *21*, 133–135.
74. Williams, I.S. Response of detrital and zircon and monazite, and their U-Pb isotopic systems, to regional metamorphism and host-rock partial melting, Cooma Complex, Southeastern Australia. *Aust. J. Earth Sci.* **2001**, *48*, 557–580, doi:10.1046/j.1440-0952.2001.00883.x.
75. Rubatto, D.; Williams, I.S.; Buick, I.S. Zircon and monazite response to prograde metamorphism in the Reynolds Range, central Australia. *Contrib. Mineral. Petrol.* **2001**, *140*, 458–468, doi:10.1007/PL00007673.
76. Fornelli, A.; Piccarreta, G.; Del Moro, A.; Acquafredda, P. Multi-stage melting in the lower crust of the Serre (southern Italy). *J. Petrol.* **2002**, *43*, 2191–2217, doi:10.1093/petrology/43.12.2191.
77. Fornelli, A.; Pascazio, A.; Piccarreta, G. Diachronic and different metamorphic evolution in the fossil Variscan lower crust of Calabria. *Int. J. Earth Sci.* **2011**, *101*, 1191–1207, doi:10.1007/s00531-011-0721-8.
78. Festa, V.; Fornelli, A.; Paglionico, A.; Pascazio, A.; Piccarreta, G.; Spiess, R. Asynchronous extension of the late-Hercynian crust in Calabria. *Tectonophysics* **2012**, *518–521*, 29–43, doi:10.1016/j.tecto.2011.11.007.
79. Fiannacca, P.; Williams, I.S.; Cirrincione, R.; Pezzino, A. Crustal contributions to late hercynian peraluminous magmatism in the Southern Calabria-Peloritani Orogen, Southern Italy: Petrogenetic inferences and the gondwana connection. *J. Petrol.* **2008**, *49*, 1497–1514, doi:10.1093/petrology/egn035.
80. Fiannacca, P.; Basei, M.A.S.; Cirrincione, R.; Pezzino, A.; Russo, D. Water-assisted production of late-orogenic trondhjemites at magmatic and subsolidus conditions. *Geol. Soc. Spec. Publ.* **2020**, *491*, doi:10.1144/SP491-2018-113.
81. Fiannacca, P.; Williams, I.S.; Cirrincione, R. Timescales and mechanisms of batholith construction: Constraints from zircon oxygen isotopes and geochronology of the late Variscan Serre Batholith (Calabria, southern Italy). *Lithos* **2017**, *277*, 302–314, doi:10.1016/j.lithos.2016.06.011.
82. Graessner, T.; Schenk, V.; Brocker, M.; Mezger, K.; Bröcker, M.; Mezger, K. Geochronological constraints on the timing of granitoid magmatism, metamorphism and post-metamorphic cooling in the Hercynian crustal cross-section of Calabria. *J. Metamorph. Geol.* **2000**, *18*, 409–421, doi:10.1046/j.1525-1314.2000.00267.x.
83. Gasquet, D.; Levresse, G.; Cheilletz, A.; Azizi-Samir, M.R.; Mouttaqi, A. Contribution to a geodynamic reconstruction of the Anti-Atlas (Morocco) during Pan-African times with the emphasis on inversion tectonics and metallogenic activity at the Precambrian-Cambrian transition. *Precambrian Res.* **2005**, *140*, 157–182, doi:10.1016/j.precamres.2005.06.009.
84. Fiannacca, P.; Williams, I.S.; Cirrincione, R.; Pezzino, A. Poly-orogenic melting of metasedimentary crust from a granite geochemistry and inherited zircon perspective (southern calabria-peloritani orogen, Italy). *Front. Earth Sci.* **2019**, *7*, 1–15, doi:10.3389/feart.2019.00119.
85. Díez Fernández, R.; Arenas, R. The Late Devonian Variscan suture of the Iberian Massif: A correlation of high-pressure belts in NW and SW Iberia. *Tectonophysics* **2015**, *654*, 96–100, doi:10.1016/j.tecto.2015.05.001.
86. Fornelli, A.; Micheletti, F.; Piccarreta, G. The Neoproterozoic-Early Cambrian felsic magmatism in Calabria

(Italy): Inferences as to the origin and geodynamic setting. *Period. Mineral.* **2007**, *76*, 99–112, doi:10.2451/2007PM0019.
87. von Raumer, J.F.; Bussy, F.; Schaltegger, U.; Schulz, B.; Stampfli, G.M. Pre-mesozoic alpine basements-their place in the European paleozoic framework. *Bull. Geol. Soc. Am.* **2013**, *125*, 89–108, doi:10.1130/B30654.1.
88. von Raumer, J.F.; Stampfli, G.M.; Arenas, R.; Sánchez Martínez, S. Ediacaran to Cambrian oceanic rocks of the Gondwana margin and their tectonic interpretation. *Int. J. Earth Sci.* **2015**, *104*, 1107–1121, doi:10.1007/s00531-015-1142-x.
89. Sandiford, M.; Powell, R. Deep crustal metamorphism during crustal extension: Modern and ancient examples. *Earth Planet. Sci. Lett.* **1986**, *79*, 151–158, doi:10.1016/0012-821X(86)90048-8.
90. Clerc, C.; Lahfid, A.; Monié, P.; Lagabrielle, Y.; Chopin, C.; Poujol, M.; Boulvais, P.; Ringenbach, J.C.; Masini, E.; De St Blanquat, M. High-temperature metamorphism during extreme thinning of the continental crust: A reappraisal of the North Pyrenean passive paleomargin. *Solid Earth* **2015**, *6*, 643–668, doi:10.5194/se-6-643-2015.
91. Stampfli, G.M.; Hochard, C.; Vérard, C.; Wilhem, C.; vonRaumer, J. The formation of Pangea. *Tectonophysics* **2013**, *593*, 1–19, doi:10.1016/j.tecto.2013.02.037.
92. Edel, J.B.; Schulmann, K.; Lexa, O.; Lardeaux, J.M. Late Palaeozoic palaeomagnetic and tectonic constraints for amalgamation of Pangea supercontinent in the European Variscan belt. *Earth-Sci. Rev.* **2018**, *177*, 589–612, doi:10.1016/j.earscirev.2017.12.007.
93. Matte, P. The Variscan collage and orogeny (480-290 Ma) and the tectonic definition of the Armorica microplate: A review. *Terra Nova* **2001**, *13*, 122–128, doi:10.1046/j.1365-3121.2001.00327.x.
94. Murphy, J.B.; Quesada, C.; Gutiérrez-Alonso, G.; Johnston, S.T.; Weil, A. Reconciling competing models for the tectono-stratigraphic zonation of the Variscan orogen in Western Europe. *Tectonophysics* **2016**, *681*, 209–219, doi:10.1016/j.tecto.2016.01.006.
95. Spiess, R.; Cesare, B.; Mazzoli, C.; Sassi, R.; Sassi, F.P. The crystalline basement of the Adria microplate in the eastern Alps: A review of the palaeostructural evolution from the Neoproterozoic to the Cenozoic. *Rend. Lincei* **2010**, *21*, 31–50, doi:10.1007/s12210-010-0100-6.
96. Stampfli, G.M.; Borel, G.D. A plate tectonic model for the Paleozoic and Mesozoic constrained by dynamic plate boundaries and restored synthetic oceanic isochrons. *Earth Planet. Sci. Lett.* **2002**, *196*, 17–33, doi:10.1016/S0012-821X(01)00588-X.
97. Di Vincenzo, G.; Carosi, R.; Palmieri, R. The Relationship between Tectono-metamorphic Evolution and Argon Isotope Records in White Mica: Constraints from in situ 40Ar-39Ar Laser Analysis of the Variscan Basement of Sardinia. *J. Petrol.* **2004**, *45*, 1013–1043, doi:10.1093/petrology/egh002.
98. Giacomini, F.; Dallai, L.; Carminati, E.; Tiepolo, M.; Ghezzo, C. Exhumation of a Variscan orogenic complex: Insights into the composite granulitic-amphibolitic metamorphic basement of south-east Corsica (France). *J. Metamorph. Geol.* **2008**, *26*, 403–436, doi:10.1111/j.1525-1314.2008.00768.x.